[CANCER RESEARCH 64, 3545–3549, May 15, 2004]

Expression of a Novel Human Gene, *Human Wings Apart-Like (hWAPL)*, Is Associated with Cervical Carcinogenesis and Tumor Progression

Kosuke Oikawa,[1,3,4] Tetsuya Ohbayashi,[1,3,4] Tohru Kiyono,[5] Hirotaka Nishi,[2] Keiichi Isaka,[2] Akihiro Umezawa,[4,6] Masahiko Kuroda,[1,3,4] and Kiyoshi Mukai[1]

Departments of [1]Pathology and [2]Obstetrics–Gynecology, Tokyo Medical University, Shinjuku-ku, Tokyo; [3]Core Research for Evolutional Science and Technology Research Project, Japan Science and Technology Corp., Kawaguchi-shi, Saitama; [4]Shinanomachi Research Park, Keio University, Shinjuku-ku, Tokyo; [5]Division of Virology, National Cancer Center Research Institute, Chuo-ku, Tokyo; and [6]National Research Institute for Child Health and Development, Setagaya-ku, Tokyo, Japan

ABSTRACT

In *Drosophila melanogaster*, the *wings apart-like* (*wapl*) gene encodes a protein that regulates heterochromatin structure. Here, we characterize a novel human homologue of *wapl* (termed *human WAPL*; *hWAPL*). The *hWAPL* mRNA was predominantly expressed in uterine cervical cancer, with weak expression in all other normal and tumor tissues examined. hWAPL expression in benign epithelia was confined to the basal cell layers, whereas in dysplasias it increasingly appeared in more superficial cell layers and showed a significant correlation with severity of dysplasia. Diffuse hWAPL expression was found in all invasive squamous cell carcinomas examined. In addition, NIH3T3 cells overexpressing hWAPL developed into tumors on injection into nude mice. Furthermore, repression of *hWAPL* expression by RNA interference induced cell death in SiHa cells. These results demonstrate that hWAPL is associated with cell growth, and the *hWAPL* expression may play a significant role in cervical carcinogenesis and tumor progression.

INTRODUCTION

The *wings apart-like* (*wapl*) gene of *Drosophila melanogaster* encodes a protein that regulates heterochromatin structure (1). Mutations of *wapl* prevent the normal close apposition of sister chromatids in heterochromatin regions but do not appear to affect either heterochromatin condensation or chromosomal segregation (1). This evidence suggests that *wapl* is required to hold sister chromatids together in mitotic heterochromatin. *wapl* has also been implicated in both heterochromatin pairing during female meiosis and the modulation of position effect variegation (1). In addition, a *P* element screen of *Drosophila* identified *wapl* as a modifier of chromosome inheritance (2).

Among all varieties of cancer, uterine cervical cancer is unique because of its association with high-risk human papillomavirus (HPV) infection, with strains like HPV-16 and HPV-18. High-risk HPVs encode two oncoproteins, E6 and E7, which subvert crucial cellular regulatory mechanisms that reactivate and maintain DNA synthesis in the host cell. E6 accelerates proteosomal degradation of the p53 tumor suppressor, and E7 inactivates the retinoblastoma protein, interfering with the action of both $p16^{INK4a}$ (3) and the cyclin-dependent kinase inhibitor $p21^{Cip1}$ (4, 5). Both the E6 and E7 high-risk HPV oncoproteins independently induce genomic instability in normal human cells (6, 7). Only a small portion of precursor lesions infected with HPV, however, develops into invasive carcinomas (8). Therefore, additional genetic and microenvironmental factors subsequent to HPV infection are thought to play an important role in the initiation and progression of cervical neoplasia (8–10).

In this study, we describe the isolation and characterization of a novel human *wapl*-related gene termed *human WAPL* (*hWAPL*). We have also demonstrated that *hWAPL* has the characteristics of an oncogene and is associated with uterine cervical cancer.

MATERIALS AND METHODS

cDNA Cloning and Construction of the hWAPL Expression Vector. To isolate the complete *hWAPL* cDNA sequence, we used a human testis Marathon-Ready cDNA kit (Clontech, Palo Alto, CA).

To create an expression vector encoding *hWAPL*, a *Hin*dIII-*Eco*RI cDNA fragment containing the complete coding region of hWAPL was amplified by PCR using the primers 5′-TTAAGCTTTGAAACTGGTGTCAAAATGACATCCAGATT-3′ and 5′-TTGAATTCAAGCAATGTTCCAAATATTCAATCACTCTAGAG-3′ and inserted into the hemagglutinin (HA)-tagged mammalian expression vector, pHM6 (HA-hWAPL; Roche Diagnostics, Mannheim, Germany).

Northern Blot and Quantitative Real-Time PCR Analysis. RNA isolation (11) and Northern blot analysis (11, 12) were performed as described. The 674-bp *Dpn*II fragment of *hWAPL* cDNA was used as a probe and labeled with ^{32}P using the Rediprime II random prime labeling system (Amersham Biosciences, Piscataway, NJ). A human β-actin cDNA control probe (Clontech) was used as a control.

First-strand cDNA synthesis was performed as described (13). Real-time PCR analysis was performed using the Smart Cycler System (Cepheid, Sunnyvale, CA) with SYBR Green I (Cambrex, Washington, DC). Real-time PCR used the *hWAPL*-specific primers 5′-GAATTCATAGGCACAGCGCTGAACTGTGTG-3′ and 5′-TTGAATTCCTAGCAATGTTCCAAATATTCA-3′ and β-actin-specific primers 5′-GGGAAATCGTGCGTGACATTAAG-3′ and 5′-TGTGTTGGCGTACAGGTCTTTG-3′. Reaction mixtures were denatured at 95°C for 30 s and then were subjected to 40 PCR cycles at 95°C for 3 s, 68°C for 30 s, and 87°C for 6 s. *hWAPL* mRNA levels were normalized to β-actin signals.

Immunohistochemistry and Immunoblot Analysis. To generate mouse monoclonal antibodies against hWAPL, we immunized mice against a 6 × histidine-tagged hWAPL COOH terminus (amino acids 814-1037) fusion protein. Spleen cells of an immunized mouse were fused with P3UI mouse myeloma cells as described previously (14). Of the 128 hybrids generated, one clone (clone R929) showed exclusive reactivity with hWAPL by ELISA. We used the supernatant of this clone as anti-hWAPL antibody.

Immunohistochemical assays were performed on formalin-fixed, paraffin-embedded sections using Ventana HX System Benchmark (Ventana Medical Systems Inc., Tucson, AZ). Immunohistochemical stains for hWAPL were interpreted semiquantitatively by assessing the intensity and extent of staining on the entire tissue sections present on the slides as described (9).

Immunoblot analyses were performed as described previously (15). The anti-HA (Roche Diagnostics; 3F10) and monoclonal anti-α-tubulin clone B-5-1-2 (Sigma Chemical Co., St. Louis, MO; T-5168) antibodies were purchased.

Animals and Treatment. BALB/cAJc1-nu female mice (4 weeks old) were purchased from Charles River Japan, Inc. (Kanagawa, Japan).

The tumorigeneicity of the stable NIH3T3 transformants overexpressing hWAPL *in vivo* was examined as described previously (16).

Cell Culture and small interfering RNA (siRNA) Transfection. SiHa and NIH3T3 cells were grown in DMEM (Sigma) containing 10% fetal bovine serum at 37°C in a 5% CO_2 environment. For the transfection of siRNA, we

Received 12/8/03; revised 3/15/04; accepted 3/16/04.

Grant support: Grant-in-Aid for Scientific Research on Priority Area (C) and Grant-in-Aid for Encouragement of Young Scientists from the Ministry of Education, Culture, Sports, Science and Technology, Japan, and a grant from Core Research for Evolutional Science and Technology, Japan Science and Technology Corp.

The costs of publication of this article were defrayed in part by the payment of page charges. This article must therefore be hereby marked *advertisement* in accordance with 18 U.S.C. Section 1734 solely to indicate this fact.

Note: T. Ohbayashi is currently at the Horizontal Medical Research Organization, Kyoto University Faculty of Medicine, Kyoto, Japan.

Requests for reprints: Masahiko Kuroda, Department of Pathology, Tokyo Medical University, 6-1-1, Shinjuku, Shinjuku-ku, Tokyo, 160-8402, Japan. Fax: 81-3-3352-6335; E-mail: kuroda@tokyo-med.ac.jp.

generated siRNAs using a Silencer siRNA Construction Kit (Ambion, Austin, TX). siRNA transfection was performed in DMEM without serum using Oligofectamine Reagent (Invitrogen Japan, Tokyo, Japan) and Opti-MEM I (Invitrogen Japan).

For cell quantitation, we harvested the cells from the wells of a 12-well plate and resuspended them in 100 μl of PBS. Trypan blue solution (100 μl, 0.4%; Sigma) was added to each sample, and viable cell numbers were quantitated using an erythrometer. The results shown are representative of three independent cell count analyses.

RESULTS

Molecular Cloning of *hWAPL*. To isolate *wapl*-related genes from human cells, we searched DNA databases and identified a cDNA fragment, KIAA0261 (17), and three expressed sequence tag clones, BE410177, BF79516, and BE257022, containing the KIAA0261 sequence. We also performed 5′ rapid amplification of cDNA ends. From these DNA sequences, we cloned and confirmed the full-length coding region sequence of the cDNA containing KIAA0261. We named this gene *hWAPL* (GenBank accession no. AB065003) to reflect its homology to *wapl*. The *hWAPL* gene product shows high sequence similarity in the WAPL-conserved region (amino acids 627-1169, 34% identical and 56% similar) and low similarity throughout the other regions to the *wapl* gene product. Several additional stretches of amino acids are also present in wapl protein (Fig. 1*A*).

High-Level Expression of hWAPL in Human Cervical Cancer. As *wapl* is involved in sister chromatid cohesion, hWAPL may modify chromosomal inheritance. Deregulation of the expression of genes involved in chromosomal inheritance directly induces a variety of disorders associated with aneuploidy, including birth defects and cancer. Northern blot analysis detected *hWAPL* mRNA expression in several invasive cervical cancer samples, examined in tandem with additional human cancers and normal tissues (Fig. 1*B*). We confirmed the *hWAPL* expression in cervical cancers by quantitative real-time PCR analysis of tumor and normal tissue samples. The levels of *hWAPL* mRNA expression in cervical cancers were significantly higher than the levels observed in either normal cervical controls or endometrial, ovarian, breast, lung, stomach, renal, and colon cancers (Fig. 1*C*).

To investigate the connection between hWAPL expression and oncogenesis in cervical malignancies, we examined the expression of hWAPL by immunohistochemistry in a series of clinical samples of the various grades of cervical dysplasia [cervical intraepithelial neoplasia (CIN) I–III] and invasive squamous cell carcinoma. We found nuclear immunostaining for hWAPL in all samples (Fig. 2*A*). hWAPL expression in benign squamous epithelia was confined to the basal and parabasal cell layers. In contrast, hWAPL expression in squamous dysplasia and invasive carcinoma increasingly appeared in the more superficial cell layers and was significantly increased compared with the adjacent benign epithelia ($P = 0.0002$ for CIN I, $P = 0.0003$ for CIN II, $P = 0.0001$ for CIN III, and $P = 0.0001$ for invasive squamous cell carcinoma; Wilcoxon's signed rank test). CIN I and II cases showed hWAPL expression in the basal 50 and 70% of the epithelial thickness, respectively, whereas CIN III and invasive squamous cell carcinoma showed hWAPL expression in the full thickness of the dysplastic epithelia (Fig. 2*A*). Furthermore, the mean hWAPL staining score increased remarkably with increasing grade of dysplasia (Fig. 2*B*). These data strongly suggest that the unscheduled high-level expression of hWAPL may play a significant role in cervical carcinogenesis and tumor progression.

hWAPL Has Oncogenic Characteristics. Because we observed high-level expression of *hWAPL* in tumors, we sought to determine whether hWAPL overexpression promotes tumor development. We transfected NIH3T3 cells with an HA-tagged hWAPL expression vector (HA-hWAPL 3T3) or HA expression vector (HA-3T3). Then, we compared the ability of HA-hWAPL 3T3 with HA-3T3 cells to grow as tumors in nude mice. We injected 10^6 cells into three s.c. sites of each nude mouse. HA-hWAPL 3T3 cells produced tumors in all nude mice within 10 days after injection of cells (100%, $n = 18$; Fig. 3*A*). HA-3T3 failed to produce tumors in any mice (0%, $n = 18$). We confirmed high hWAPL expression levels in the resultant tumors by Western blot analysis (Fig. 3*B*). These results suggest that *hWAPL* has the characteristics of an oncogene.

Repression of hWAPL Expression Induces Cell Death. We examined hWAPL function by suppressing hWAPL expression. Initial attempts to generate a *WAPL*-deficient mouse demonstrated that the loss of *WAPL* was embryonic lethal (data not shown). Therefore, we designed two 21-nucleotide, double-stranded siRNAs, siRNA(I) and siRNA(II), to repress *hWAPL* expression (Refs. 18 and 19; Figs. 1*A*

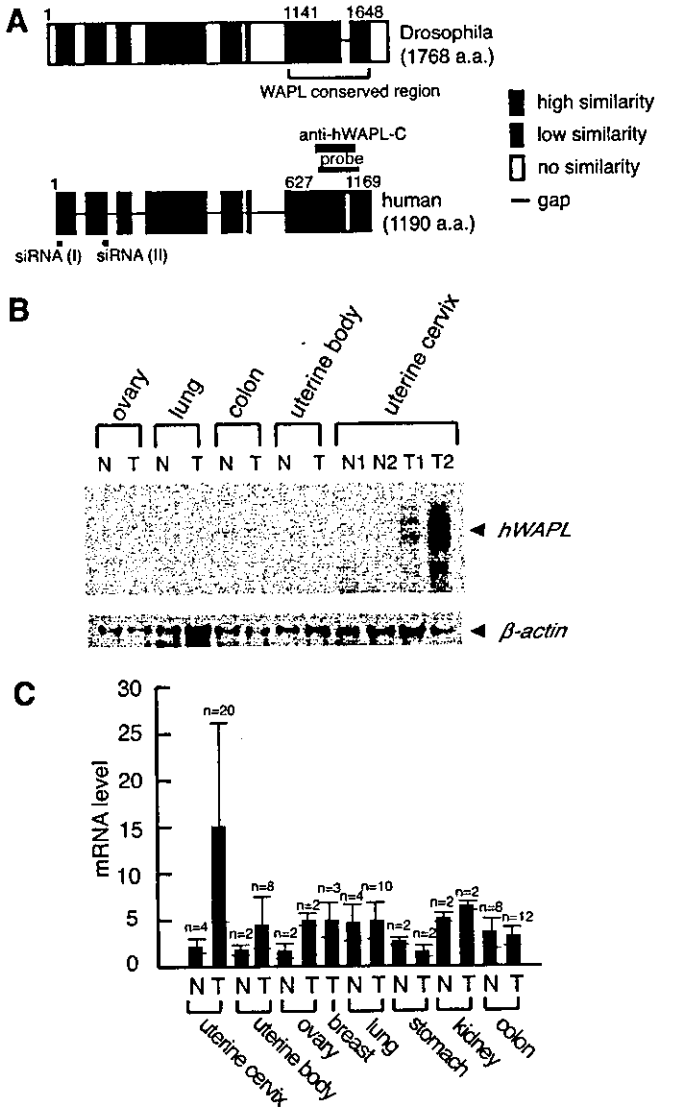

Fig. 1. Structures of wings apart-like (*WAPL*) proteins and *human WAPL* (*hWAPL*) expression in normal and tumor human tissues. *A*, schematic structure of the *hWAPL* and *Drosophila wapl* gene products. The site corresponding to the probe sequence used for Northern blot analysis is indicated by "probe." The antibody recognition site is indicated by "hWAPL-C." The small interfering RNA (*siRNA*) targeting sites are indicated by "siRNA(I)" and "siRNA(II)." *B*, Northern blot analysis of *hWAPL* in several normal (*N*) and tumor (*T*) human tissues. *C*, quantitative real-time PCR analysis demonstrating *hWAPL* mRNA levels in various normal (*N*) and tumor (*T*) human tissues. *Columns*, the means of examined samples. The minimum mRNA expression level was arbitrarily set to 1 in the graphical presentation; all other mRNA signals were normalized to this value. *Bars*, SD.

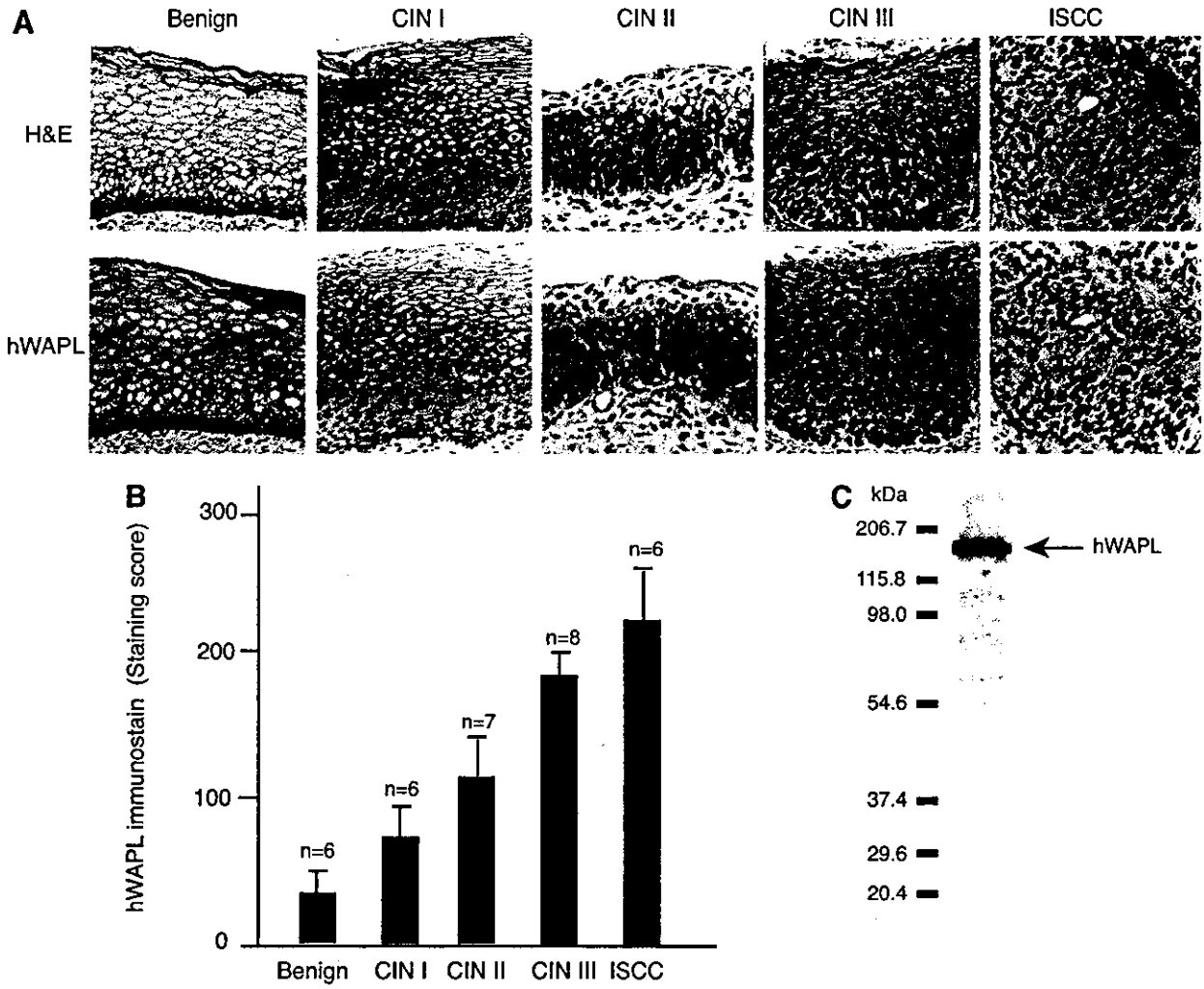

Fig. 2. Immunohistochemical analysis of human wings apart-like (*hWAPL*) expression in uterine cervical epithelia of normal, dysplasia, and carcinoma. *A*, immunohistochemical staining of hWAPL expression in benign squamous epithelium, various grades of squamous dysplasia [cervical intraepithelial neoplasia (*CIN*) grades I, II, and III], and invasive squamous cell carcinoma (*ISCC*). hWAPL was stained with hematoxylin counterstain; H&E. *B*, graphical representation of the increase of the hWAPL expression with increasing severity of dysplasia in cervical squamous epithelia. The mean hWAPL staining scores were calculated as described (9). *Bars*, SD. *C*, Western blot analysis with the total extract from a uterine cervical cancer-derived cell line, SiHa, to confirm the specificity of the anti-hWAPL monoclonal antibody hWAPL-C.

and 4*A*). We examined various human cancer-derived cell lines and found that cervical cancer-derived cell lines containing both HPV-positive and -negative cells exhibited higher levels of hWAPL expression compared with the other cell lines (data not shown). Then, we examined the effects of suppressing *hWAPL* in a cervical cancer-derived cell line, SiHa. siRNA transfection at a concentration of either 1 nM siRNA(I) or siRNA(II) reduced *hWAPL* mRNA levels (Fig. 4*B*). siRNA(I) was more effective at reducing *hWAPL* mRNA than siRNA(II). Thus, we used siRNA(I) in the subsequent experiments. hWAPL protein levels were also significantly reduced after siRNA(I) transfection (Fig. 4*C*). Interestingly, siRNA(I) repressed the growth of the cells and subsequently induced cell death (Fig. 4, *D* and *E*). siRNA(II) repressed cell growth in a similar manner as siRNA(I) (Fig. 4*D*), suggesting that the effects of these siRNAs on proliferation and viability are likely caused by the repression of *hWAPL* expression. Similar results were obtained in another cervical cancer-derived cell line, CaSki, with 10 nM siRNA(I) (data not shown). On the contrary, we did not observe any effects of siRNA(I) on cells expressing relatively low levels of *hWAPL*, such as Saos-2 and HCT116 (data not shown).

To investigate the fate of cells transfected with siRNA(I), we analyzed siRNA-transfected cells by flow cytometry (Fig. 5). In siRNA(I)-transfected cells, the population of cells exhibiting S phase DNA content increased (Fig. 5; 48 and 72 h). In addition, there was an increase in the number of apoptotic cells exhibiting subG$_1$ DNA content (Fig. 5; 72 h). Many cells showing S phase DNA content may also be apoptotic cells at G$_2$-M phase. Taken together, these results suggest that a malfunction in the hWAPL pathway activates an S phase checkpoint or another apoptotic pathway and consequently leads to cell death.

DISCUSSION

In this study, we report the isolation and characterization of a novel human gene termed *hWAPL*. We were unable to identify additional genes similar to *wapl* within the human genome sequence database. Thus, although the high-sequence conservation between hWAPL and wapl is limited to a third of the protein sequence encoded by *wapl* (Fig. 1*A*), we consider hWAPL to be the human homologue of wapl. We did not find any protein sequence motifs in hWAPL, except for the WAPL-conserved region (Fig. 1*A*). We therefore expect that hWAPL has similar functions to the wapl protein. Two hybridization signals for *hWAPL* were visible by Northern blot analysis (Fig. 1*B*). Western blot analysis, however, detected only a single band for

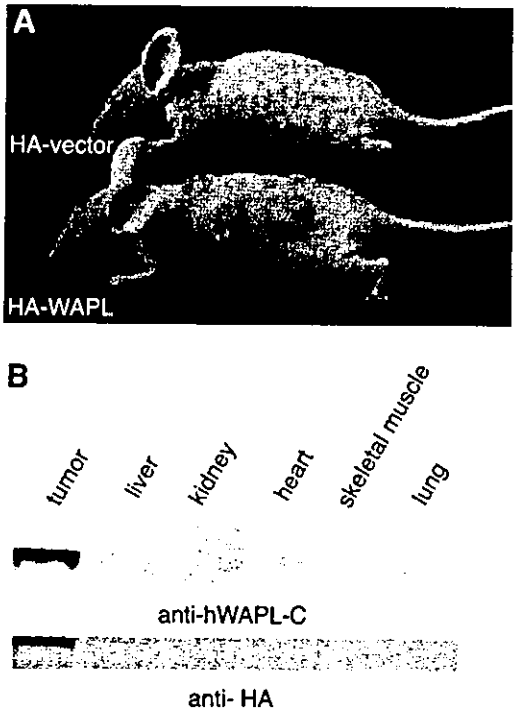

Fig. 3. Human wings apart-like (*hWAPL*) overexpression promotes tumor development. *A*, tumorigenecity of HA-hWAPL 3T3 in nude mice. The lower mouse in the *panel* is shown 10 days after the injection of HA-hWAPL-3T3 at three s.c. sites. The upper mouse was injected with the control HA-3T3 cells. *B*, Western blot analysis of hWAPL protein in tumor and other control tissues from HA-hWAPL-3T3-injected nude mice. *Top panel*, anti-hWAPL antibody; *bottom panel*, anti-HA antibody.

hWAPL (Fig. 2*C*). In addition, we did not obtain additional nucleotide sequences similar to the open reading frame of *hWAPL* by PCR analysis with various PCR primers (data not shown). Thus, we consider that the two hybridization signals may reflect the difference of the length of the untranslated regions of the *hWAPL* mRNA.

High-level expression of *hWAPL* was observed in cervical cancers (Fig. 1, *B* and *C*). Furthermore, hWAPL-overexpressing 3T3 cells developed into tumors on injection into nude mice (Fig. 3). These results suggest that *hWAPL* has oncogenic characteristics. Cervical cancer is a serious health problem, with ~500,000 women developing the disease each year worldwide. In many developing countries, it is the most common cause of cancer death and years of life lost because of cancer (20). Although the fundamental role of high-risk HPV infection in the pathogenesis of cervical carcinoma is well established, other factors are thought to play a role in cervical carcinogenesis (8, 21). Because all of uterine cervical samples examined were HPV positive (data not shown), it is still to be confirmed whether hWAPL expression is inducible by HPV infection. However, HPV-positive normal cervical tissue samples exhibited low hWAPL expression (Fig. 1, *B* and *C* and data not shown), and an HPV-negative, uterine cervical cancer-derived cell line, C33A, showed high hWAPL expression (data not shown). Thus, hWAPL expression is likely to be more closely related with cervical carcinogenesis than HPV infection. Recently, Acs *et al.* (9) found significant correlation among expression of Epo receptor, $p16^{INK4a}$, and *bcl*-2 in benign and dysplastic squamous epithelia. In our results, hWAPL showed similar expression pattern to Epo receptor and $p16^{INK4a}$ in benign and dysplastic cervical squamous epithelia and invasive squamous cell carcinomas (Fig. 2, *A* and *B*). Although we did not find any evidence for hWAPL being involved in hypoxia-inducible Epo signaling, hWAPL may cooperate with the Epo signaling in the progression of cervical neoplasia. These observations indicate that hWAPL overexpression can be used as a useful diagnostic tool in the detection of cervical dysplasia like $p16^{INK4a}$ (22) and Epo receptor (9). In addition, our results provide the necessity to investigate the potential of hWAPL as a cancer therapeutic target.

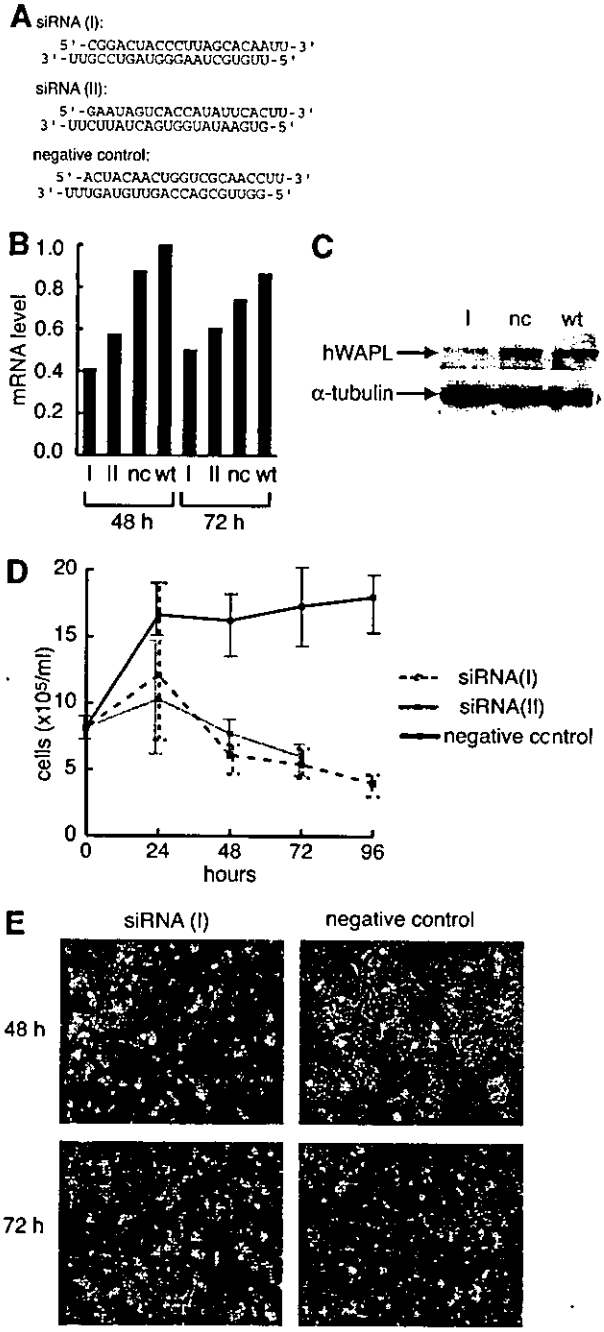

Fig. 4. Repression of human wings apart-like (*hWAPL*) expression by small interfering RNA (*siRNA*) treatment induces cell death. *A*, sequences and structures of siRNAs. The negative control siRNA possesses the same nucleotide composition as siRNA(I) but lacks homology to any known human genes. *B*, reduction of the *hWAPL* transcript by siRNA in SiHa cells. After siRNA transfection, SiHa cells were harvested at either 48 or 72 h. Total RNA was extracted from the cells and subjected to real-time PCR analysis. *I*, siRNA(I); *II*, siRNA(II); *nc*, negative control siRNA; *wt*, untransfected wild type. Data were normalized to a maximum mRNA level that was arbitrarily set to 1 in the graphical presentation. *C*, reduction of hWAPL protein levels by siRNA. Western blot analysis of total cell extracts from untreated SiHa or SiHa cells 72 h after transfection with siRNA(I) or negative control siRNA. α-tubulin is shown as a loading control. *D*, active siRNA specific for *hWAPL* induces cell death. SiHa cells transfected with siRNA(I), siRNA(II), or negative control siRNA were harvested at 24, 48, 72, and 96 h after transfection. Cell numbers were counted using an erythrometer. *Bars*, SE. *E*, representative phase-contrast images of SiHa cells transfected with siRNA(I) and negative control siRNA are shown.

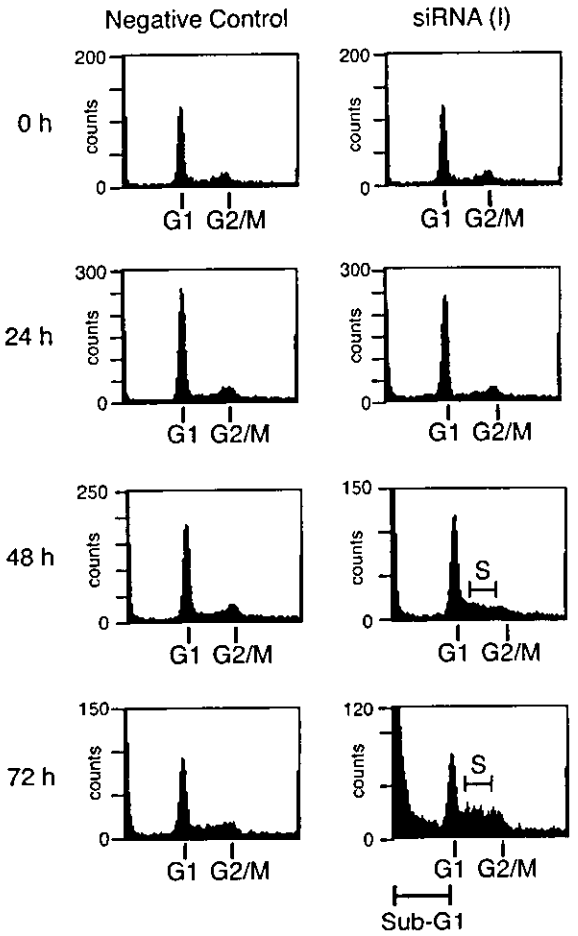

Fig. 5. Flow cytometric analysis of SiHa cells after small interfering RNA (*siRNA*) transfection. SiHa cells were transfected with either siRNA(I) or negative control siRNA, then harvested at 24, 48, and 72 h after transfection. Cells were stained with propidium iodide and subjected to flow cytometric analysis to examine DNA content. A total of 50,000 cells was counted for the sample siRNA(I) 72 h, and 20,000 cells were counted for the other samples.

Loss of WAPL was embryonic lethal in mouse (data not shown), and repression of hWAPL expression in SiHa cells led to cell death (Fig. 4). Flow cytometry analysis demonstrated that malfunction of hWAPL may cause apoptosis and/or arrest of cells at S phase (Fig. 5). In addition, *Drosophila wapl* is associated with regulation of chromatin organization (1). Thus, we expect that hWAPL is also associated with regulation of chromatin structure, and deregulation of hWAPL expression may induce chromosomal instability. Although additional investigations are necessary to elucidate the actual function of hWAPL in normal and malignant cells, our results have demonstrated that the novel oncogene, *hWAPL*, is one of the essential genes for development and cell growth and may play a significant role for cervical carcionogenesis and tumor progression.

ACKNOWLEDGMENTS

We thank K. Yoshida, R. Iwata, R. Tsujimoto, K. Kitamura, M. Sugiura, and M. Takaoka for their technical assistance.

REFERENCES

1. Verni F, Gandhi R, Goldberg ML, Gatti M. Genetic and molecular analysis of wings apart-like (wapl), a gene controlling heterochromatin organization in Drosophila melanogaster. Genetics 2000;154:1693–710.
2. Dobie KW, Kennedy CD, Velasco VM, et al. Identification of chromosome inheritance modifiers in Drosophila melanogaster. Genetics 2001;157:1623–37.
3. Kiyono T, Foster SA, Koop JI, McDougall JK, Galloway DA, Klingelhutz AJ. Both Rb/p16^{INK4a} inactivation and telomerase activity are required to immortalize human epithelial cells. Nature 1998;396:84–8.
4. Jones DL, Alani RM, Munger K. The human papillomavirus E7 oncoprotein can uncouple cellular differentiation and proliferation in human keratinocytes by abrogating p21^{Cip1}-mediated inhibition of cdk2. Genes Dev 1997;11:2101–11.
5. zur Hausen H. Papillomavirus infections–a major cause of human cancers. Biochim Biophys Acta 1996;1288:F55–78.
6. Hashida T, Yasumoto S. Induction of chromosome abnormalities in mouse and human epidermal keratinocytes by the human papillomavirus type 16 E7 oncogene. J Gen Virol 1991;72:1569–77.
7. White AE, Livanos EM, Tlsty TD. Differential disruption of genomic integrity and cell cycle regulation in normal human fibroblasts by the HPV oncoproteins. Genes Dev 1994;8:666–77.
8. Milde-Langosch K, Riethdorf S, Loning T. Association of human papillomavirus infection with carcinoma of the cervix uteri and its precursor lesions: theoretical and practical implications. Virchows Arch 2000;437:227–33.
9. Acs G, Zhang PJ, McGrath CM, et al. Hypoxia-inducible erythropoietin signaling in squamous dysplasia and squamous cell carcinoma of the uterine cervix and its potential role in cervical carcinogenesis and tumor progression. Am J Pathol 2003; 162:1789–806.
10. Schiffman MH, Brinton LA. The epidemiology of cervical carcinogenesis. Cancer 1995;76:1888–901.
11. Oikawa K, Ohbayashi T, Mimura J, et al. Dioxin suppresses the checkpoint protein, MAD2, by an aryl hydrocarbon receptor-independent pathway. Cancer Res 2001;61: 5707–9.
12. Sok J, Wang XZ, Batchvarova N, Kuroda M, Harding H, Ron D. CHOP-dependent stress-inducible expression of a novel form of carbonic anhydrase VI. Mol Cell Biol 1999;19:495–504.
13. Kuroda M, Ishida T, Takanashi M, Satoh M, Machinami R, Watanabe T. Oncogenic transformation and inhibition of adipocytic conversion of preadipocytes by TLS/FUS-CHOP type II chimeric protein. Am J Pathol 1997;151:735–44.
14. Kuroda M, Horiuchi H, Ono A, Kawakita M, Oka T, Machinami R. Immunohistochemical study on the distribution of sarcoplasmic reticulum calcium ATPase in various human tissues using novel monoclonal antibodies. Virchows Arch A Pathol Anat Histopathol 1992;421:527–32.
15. Oikawa K, Ohbayashi T, Mimura J, et al. Dioxin stimulates synthesis and secretion of IgE-dependent histamine-releasing factor. Biochem Biophys Res Commun 2002; 290:984–7.
16. Kuroda M, Wang X, Sok J, et al. Induction of a secreted protein by the myxoid liposarcoma oncogene. Proc Natl Acad Sci USA 1999;96:5025–30.
17. Nagase T, Seki N, Ishikawa K, et al. Prediction of the coding sequences of unidentified human genes. VI. The coding sequences of 80 new genes (KIAA0201-KIAA0280) deduced by analysis of cDNA clones from cell line KG-1 and brain. DNA Res 1996;3:321–9, 41–54.
18. Hannon GJ. RNA interference. Nature 2002;418:244–51.
19. McManus MT, Sharp PA. Gene silencing in mammals by small interfering RNAs. Nat Rev Genet 2002;3:737–47.
20. Waggoner SE. Cervical cancer. Lancet 2003;361:2217–25.
21. Park TW, Fujiwara H, Wright TC. Molecular biology of cervical cancer and its precursors. Cancer 1995;76:1902–13.
22. Klaes R, Friedrich T, Spitkovsky D, et al. Overexpression of p16^{INK4a} as a specific marker for dysplastic and neoplastic epithelial cells of the cervix uteri. Int J Cancer 2001;92:276–84.

Pathology International 2004; **54**: 26–31

Original Article

Human DNA damage checkpoints and their relevance to soft tissue sarcoma

Hiroyuki Hattori,[1] Masahiko Kuroda,[2] Tsuyoshi Ishida,[2] Koutarou Shinmura,[1] Shuzou Nagai,[1] Kiyoshi Mukai[2] and Atsuhiro Imakiire[1]

[1]*Department of Orthopedic Surgery and* [2]*First Department of Pathology, Tokyo Medical University, Tokyo, Japan*

Soft tissue sarcoma (STS) is a malignant neoplasm, arising in mesenchymal tissues, that is difficult to treat clinically because it can be highly resistant to chemo-radiotherapy. At present, the mechanism of that resistance remains unclear. Cell cycle checkpoints engender strict control of cell proliferation, arresting the cell cycle to provide time for repair or apoptosis when DNA damage is induced by unprogrammed extrinsic events. These pathways involve at least two checkpoints: one at the G1/S transition and one at the G2/M transition. The *p53* gene, which is mutated in several malignant tumors, plays an important role in DNA repair at the G1/S transition; however, there is little information on the G2/M checkpoint in STS. In the present study, several proteins (phospho-p53, -cdc25, -cdc2, -Chk1 and -Chk2) involved in checkpoint pathways were investigated using immunohistochemistry in STS specimens. Most STSs maintain a well-preserved G2/M checkpoint despite the loss of the G1/S checkpoint (phospho-p53: 4.9% (2/41); -cdc25: 41% (17/41); -cdc2: 61% (25/41); -Chk1: 29% (12/41); -Chk2: 46% (19/41)). Furthermore, in a postoperative chemotherapy case the number of cells positive for phospho-cdc25 and -Chk2 was higher in a recurrent tumor than in the primary tumor ($n = 7$, $P = 0.046 < 0.05$, Wilcoxon signed-ranks test). These findings indicate that the G2/M checkpoint pathway is well preserved and might contribute to the chemotherapeutic resistance associated with STS.

Key words: chemotherapy, DNA-damage checkpoint, soft tissue sarcoma

Soft tissue sarcomas (STS) are a heterogeneous group of malignant neoplasms that can arise from mesenchymal lineages anywhere in the body. Clinically, radical surgical resection is the mainstay of treatment for adult STS because these neoplasms are highly resistant to chemo-radiotherapy. Thus, successful treatment of STS is often difficult and the molecular mechanism of the chemo-radiotherapy resistance of STS remains to be elucidated.

Genetic instability, which is an essential factor in the development of most malignant tumors, often involves the gain and/or loss of whole chromosomes or translocations, leading to aneuploidy. Recent studies have revealed that the loss of function of cell cycle checkpoints contributes to genetic instability in malignant tumors.[1–3] When DNA damage is induced by unprogrammed extrinsic events, cell cycle checkpoints are activated and exercise strict control of cell proliferation, arresting growth to provide time for repair and apoptosis.[4] It has been well established that there are two cell cycle checkpoints: one at G1/S and the other at G2/M. The p53 gene product plays a central role in DNA repair at the G1/S checkpoint. The induction of *p53* results in transcriptional activation of the p16-cyclin D1/cdk4-Rb pathway, GADD45, and MDM2, and leads to either cellular arrest in G1 or apoptosis.[1] Failure of these pathways has been detected in several malignant tumors,[5,6] and *p53* mutations have been detected in approximately 20% of STS. An additional 40–60% of STS exhibit p53 protein overexpression.[7,8]

Although our knowledge of the G2/M checkpoint is still incomplete, a few proteins in this pathway have been identified. The cell cycle checkpoint kinases Chk1 and Chk2 act downstream of ATM in the DNA damage response at the G2/M transition. In the presence of damaged DNA, both Chk1 and Chk2 phosphorylate and inactivate cdc25, which in turn mediates the G2 cyclin-dependent kinase complex, resulting in G2 arrest and prevention of the initiation of mitosis.[9,10] In addition, it has been reported that p53 protein is also required in the G2/M checkpoint in human cells.[11] The failure of this pathway has been detected in a few malignant tumors, including colorectal cancer, lung cancer and some tumors of Li–Fraumeni Syndrome patients.[12–14] These mutations are associated with genetic instability; however, dysfunction of the G2/M checkpoint has been found to be relatively infrequent. Although some

Correspondence: Masahiko Kuroda, MD, First Department of Pathology, Tokyo Medical University, 6-1-1, Shinjuku, Shinjuku-ku, Tokyo 160-8402, Japan. Email: kuroda@tokyo-med.ac.jp

Received 24 June 2003. Accepted for publication 19 September 2003.

information about the G2/M checkpoint has been elucidated, studies of this checkpoint in STS have been particularly sparse.

Considering that chemotherapeutic agents cause cell death by introducing severe DNA damage to cells, the G2/M checkpoint is likely to be important for the biological behavior and treatment of *p53*-mutant tumors such as STS. For this reason, the aim of this study was to investigate the presence and function of the G2/M checkpoint proteins in STS tissue specimens, and how these tumors react to the DNA damage inflicted by chemotherapy.

MATERIALS AND METHODS

Tumor samples and histological subtype

Samples were collected at the Tokyo Medical University Hospital. As shown in Table 1, there were 31 cases of STS of which 28 were primary and 13 locally recurrent tumors, giving a total of 41 individual tumor samples. The mean age of the patients was 46.7 years (range, 5–82 years). 17 patients were male and 14 were female. None of the patients had received preoperative radiotherapy or chemotherapy, and all of them underwent surgical therapy with tumor-free resection margins.

Table 1 Clinicopathological features of soft tissue sarcomas

	Primary (n=28)	Recurrence (n=13)
Sex (No. cases)		
Male	17	6
Female	11	7
Age (years), mean	46.6	23
Site		
Lower	20	8
Upper	0	0
Trunk	8	5
Postoperative chemotherapy (No. cases)	14	13
Histopathology (No. cases)		
LPS	10	5
SS	5	4
MFH	4	1
LMS	3	2
Others	6	1

LPS, liposarcoma; LMS, leiomyosarcoma; MFH, malignant fibrous histocytoma; SS, synovial sarcoma.

Fourteen patients (50%) received postoperative chemotherapy for the primary tumor, using several protocols of combination chemotherapies (2–4 agents: doxorubicin, vincristine, cyclophosphamide, dacarbazine and ifosfamide). Treatments were given in a median total of four courses (range, 3–10 courses). Seven of the 14 patients (50%) had at least one episode of recurrence.

The median follow-up for the patients was 29 months (range, 3–92 months). From the 31 STS patients, we investigated 10 liposarcomas, six synovial sarcomas, five leiomyosarcomas, four malignant fibrous histocytomas, two Ewing's sarcomas, two malignant peripheral nerve sheath tumors, one alveolar soft part sarcoma and one spindle cell sarcoma.

Immunohistochemistry

Anti-activated p53, Chk1, and Chk2 and anti-inactivated cdc25 and cdc2 were used for the immunohistochemical assays (Table 2). Anti-phospho-p53 (Ser15) monoclonal antibody (clone 16G8) detects p53 only when it is phosphorylated at serine 15 and does not react with unphosphorylated p53. Anti-phospho-cdc25 (Ser216) monoclonal antibody detects only phosphorylated cdc25. Anti-phospho-cdc2 (Tyr15) antibody detects cdc2 and cdk2 only when they are phosphorylated at tyrosine 15.[15] This antibody does not cross-react with cdk4, cdk6 or cdk7. Anti-phospho-Chk1 (Ser345) antibody detects Chk1 only when it is phosphorylated at serine 345 and does not cross-react with other proteins.[16] Anti-phospho-Chk2 (Thr68) antibody detects Chk2 only when it is phosphorylated at threonine 68 and does not react with unphosphorylated Chk2. These antibodies were purchased from Cell Signaling Technology (MA, USA). Tonsil, mammary gland and spinal cord tissues were used as controls for these antibodies.

Tissue specimens were fixed with 10% v/v formalin, embedded in paraffin and then 4 μm sections were cut, placed on glass slides, and deparaffinized. The slides were treated with 3% H_2O_2 in 50% methanol for 20 min to eliminate endogenous peroxidase activity, and were then heated in 10 mmol/L citrate buffer (pH 6.0) for 10 min using an autoclave for antigen retrieval.

For immunohistochemical staining of phospho-p53 (Ser15) and phospho-cdc25 (Ser216), the labeled streptavidin biotin

Table 2 Antibodies and methods of immunohistochemistry

Antibodies to	Antibody type	Phosphorylated site	Method
Phospho-p53	Mouse monoclonal IgG1	Serine15	LSAB
Phospho-cdc25	Mouse monoclonal	Serine 216	LSAB
Phospho-cdc2	IgG2a	Tyrosine15	CSA
Phospho-Chk1	Rabbit polyclonal IgG	Serine345	CSA
Phospho-Chk2	Rabbit polyclonal IgG	Threonine68	CSA

CSA, catalyzed signal amplification; LSAB, labeled streptavidin–biotin method.

(LSAB) method was used. The primary antiphospho-p53, and -cdc25 antibodies were used at dilutions of 1:50 and 1:100, respectively, and slides were incubated with diluted antibody in a humidified chamber at room temperature overnight. Thereafter, the slides were incubated with biotinylated antirabbit IgG for 30 min, followed by incubation with horseradish peroxidase-labeled streptavidin for 30 min (LSAB Kit, DAKO Carpinteria, CA, USA). The immunoreaction was visualized using 2% 3,3'-diaminobenzidine (DAB) and 0.02% H_2O_2 in 0.05 mol/L Tris-buffer (Tris) for 3–5 min, after which the slides were counterstained with hematoxylin. The slides were incubated for 3 min in three fresh baths of Tris between each reaction step.

The catalyzed signal amplification (CSA) method was used for the immunostaining of phospho-cdc2 (Tyr15), phospho-Chk1 (Ser345) and phospho-Chk2 (Thr68). Briefly, the slides were incubated with avidin solution for 10 min, then biotin solution for 10 min to block endogenous biotin (Biotin Blocking System, DAKO). Next, the slides were incubated with a protein block to suppress non-specific binding of subsequent reagents, followed by incubation with the primary antibodies. The primary antiphospho-cdc2, Chk1, and Chk2 antibodies were used at dilutions of 1:100, 1:100 and 1:1000, respectively, and the slides were incubated with diluted antibody for 15 min. Antibody incubations were followed by sequential 15-min incubation with biotinylated link antibody, streptavidin-biotin-peroxidase complex, biotinyl tyramide (amplification reagent), and streptavidin peroxidase (CSA System, DAKO). Staining was completed with a 3–5-min incubation with DAB and H_2O_2 in Tris, after which the slides were counterstained with hematoxylin. For further suppression of background staining, slides were incubated for 3 min in three fresh baths of 0.1% Triton X-100 in Tris (TBS) between each reaction step.

Three fields were examined (×50) and the results were expressed by the estimated percentage of tumor cells (%) using the Win Roof Ver3.54 image analysis system (Mitani Co., Japan).

Statistical analysis

The two sample Student's *t*-test was used for data that showed equal variance. When the data showed unequal variance, Mann–Whitney's *U*-test and Wilcoxon signed-ranks test were used. A *P*-value of less than 0.05 was considered to be statistically significant.

RESULTS

G1/S checkpoint

We performed immunohistochemical analysis on tumor samples with the antiphospho-p53 antibody (Table 3). We designated cytoplasmic staining for phospho-p53 as indicating p53 was inactive and nuclear staining indicating p53 was functionally activated.

Nine of the 28 (32%) primary STS specimens and eight of the 13 (44%) recurrent tumors demonstrated positive staining of p53 in the tumor cell cytoplasm (Fig. 1a). Positive nuclear staining was observed in only two of the 28 (7.1%) primary specimens (Fig. 1b). In the recurrent tumor specimens, none of the 13 showed nuclear staining of the tumor cells. In all, only 4% (2/41) of the STS showed positive nuclear staining for phospho-p53.

G2/M checkpoint

We next examined the G2/M checkpoint using antiphospho-cdc25, -cdc2, -Chk1 and -Chk2 antibodies (Table 3). cdc25 is phosphorylated throughout interphase, but not during mitosis. Phosphorylated cdc25 binds to members of the 14-3-3 family of proteins, and is exported from the nucleus to the cytoplasm. Graves *et al.* proposed that cdc25 is actively exported from the nucleus by 14-3-3 binding, and a mutant of cdc25 that is unable to bind to 14-3-3 accumulates in the nucleus.[18] Therefore, we reasoned that cytoplasmic phospho-cdc25 staining would demonstrate an activated G2/M checkpoint. Nine of the 28 (32%) primary specimens and eight of the 13 (44%) recurrent specimens showed cytoplasmic phospho-cdc25 staining (Fig. 1c).

cdc2 is negatively regulated during interphase and in response to G2/M checkpoint activation; it is regulated by changes in subcellular localization. Throughout interphase, cdc2/cyclinB complexes (phosphorylated cdc2-cyclinB) shuttle between the nucleus and cytoplasm. We therefore rea-

Table 3 Summary of immunohistochemistry

Antigen	Staining pattern	Primary site	Recurrent site
Phospho-p53	Cytoplasm staining	32.0% (9/28)	44.0% (8/13)
	Nuclear staining	7.1% (2/28)	0% (0/13)
Phospho-cdc25	Nuclear staining	32.0% (9/28)	44.0% (8/13)
Phospho-cdc2	Nuclear and cytoplasm staining	54.0% (15/28)	77.0% (10/13)
Phospho-Chk1	Nuclear stanining	21.0% (6/28)	46.0% (6/13)
Phospho-Chk2	Nuclear staining	39.0% (11/28)	62.7% (8/13)

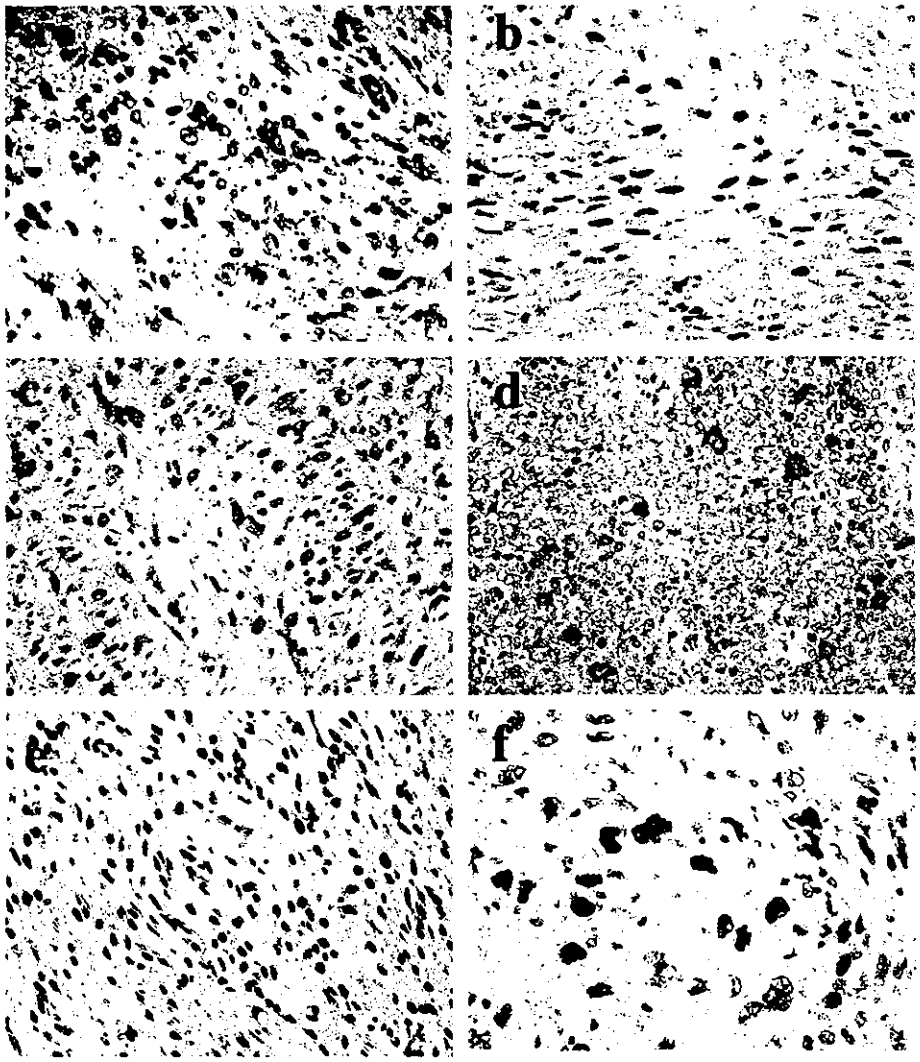

Figure 1 Immunohistochemical analysis of phospho-p53, -cdc25, -cdc2, -Chk1 and -Chk2. Positive signal is visualized as brown staining. Hematoxylin was used for counterstaining. (**a**) Phospho-p53 cytoplasmic staining of the tumor cells, without nuclear staining, in a pleomorphic liposarcoma. (**b**) Phospho-p53 nuclear staining in a malignant peripheral nerve sheath tumor can be seen in a small percentage of the tumor cells. (**c**) Phospho-cdc25 cytoplasmic staining in a pleomorphic liposarcoma can be seen as a focal component of the tumor cells. (**d**) Phospho-cdc2 immunoreactivity in a Ewing's sarcoma is nuclear as well as cytoplasmic. (**e**) Phospho-Chk1 nuclear staining in a myxoid liposarcoma. (**f**) Phospho-Chk2 nuclear staining in a malignant fibrous histocytoma.

soned that phospho-cdc2 staining of both the cytoplasm and nucleus was a sign of an activated G2/M checkpoint. Fifteen of the 28 (54%) primary specimens and 10 of the 13 (77%) recurrent specimens stained positive for phospho-cdc2 in the nucleus and cytoplasm (Fig. 1d).

Chk1 and Chk2 are kinases downstream of ATM and both have a important role in the G2/M checkpoint. These proteins are phosphorylated in the nucleus and activated in response to DNA damage. They can inactivate cdc25 via phosphorylation at serine 216, blocking the activation of cdc2 and transition into M-phase. Six of the 28 (21%) primary specimens and six of the 13 (46%) recurrent specimens stained positive for nuclear phospho-Chk1 (Fig. 1e). Eleven of the 28 (39%) primary specimens and eight of the 13 (62%) recurrent specimens stained positive for phospho-Chk2 in the nucleus (Fig. 1f).

These findings strongly suggest that most STS had a well-preserved and activated G2/M checkpoint (activated Chk1 and Chk2, inactivated cdc25 and cdc2).

Correlation of G2/M checkpoint activity between primary and recurrent tumors

Phospho-cdc25, -Chk1 and -Chk2 positivity rates (%) were compared in the primary and recurrent tumors ($n = 41$), but there were no correlations ($P = 0.142$, $= 0.516$, $= 0.197$ >0.05, Student t-test).

Influence of chemotherapy on the G2/M checkpoint

To address the question of whether intact checkpoints may have an effect on the chemo-radiotherapeutic resistance of STS, we examined postoperative chemotherapy cases ($n = 14$) and the development of subsequent recurrence ($n = 7$). The phospho-cdc25, Chk1 and -Chk2 positivity rates in the primary site did not significantly predict local recurrence ($P = 0.479$, 0.596 and $0.261 > 0.05$, Mann–Whitney's U-test).

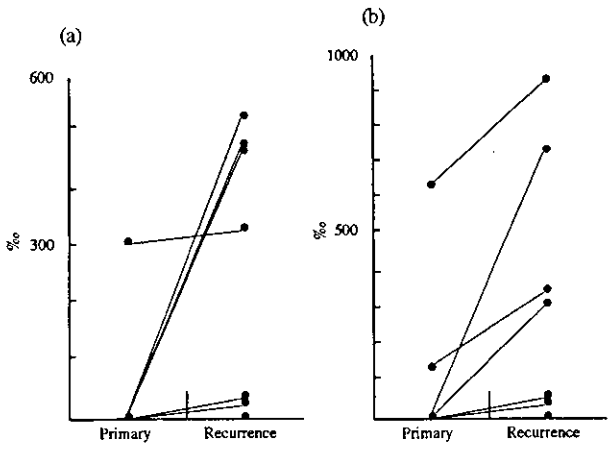

Figure 2 Correlation of (a) phospho-cdc25 and (b) phospho-Chk2 positivity between primary and recurrent tumors. Rates of both phospho-cdc25 and -Chk2 positivity are increased in the recurrent tumors relative to the primaries in the same patient ($n = 7$) in cases of postoperative chemotherapy (Wilcoxon signed-rank test). (a) $P = 0.046 < 0.05$; (b) $P = 0.046 < 0.05$.

Next, we compared the positivity rates in the primary and recurrent tumors of the cases of recurrence after postoperative chemotherapy ($n = 7$). Both the phospho-cdc25 and -Chk2 positivity rates of the primary tumors were more significantly increased than the recurrent ones ($P = 0.04 < 0.05$, Wilcoxon signed-ranks test) (Fig. 2). ($P = 0.046 < 0.05$, Wilcoxon signed-ranks test) (Fig. 2).

DISCUSSION

We have demonstrated through immunohistochemical analysis that the G2/M checkpoint is well preserved and activated in STS despite the loss of the G1/S checkpoint. In addition, positive staining for both phospho-cdc25 and -Chk2 was higher in the recurrent tumors than in the primary ones in postoperative chemotherapy cases. Many malignant tumor therapeutic agents, such as combination chemotherapy, cause cell death by causing severe DNA damage to tumor cells. We hypothesized that STS survival leading to recurrence after postoperative chemotherapy would depend on the G2/M checkpoint. Our results suggested that the damage to the cellular DNA caused by chemotherapeutic agents activated the G2/M checkpoint pathway, enabling the tumor cells to put up a strong resistance to cytotoxic agents. Because G1/S checkpoint-defective tumor cells can only repair DNA in the G2 phase, abrogation of the G2/M checkpoint might be expected to increase the sensitivity to DNA-damaging reagents more profoundly in tumor cells than normal cells.[19,20] Hartwell and Kastan noted that cancer cell survival after chemotherapy or radiotherapy depended on the specific checkpoint or repair pathways that had been lost and therefore how susceptible the cells were to these treatments.[1] Moreover, caffeine-assisted chemotherapy has been reported as advantageous in the treatment of malignant tumors,[19–22] and a recent study suggests that caffeine abrogates the G2/M checkpoint by targeting the ATM-Chk2 pathway (it prevents the Ser216 phosphorylation of cdc25).[23] We hypothesize that one of the critical checkpoint pathways is the G2/M checkpoint (CHK-cdc25-cdc2), and that there would be some therapeutic potential gained by targeting these pathways in STS.

How do we deal with STS in which the G2/M checkpoint is activated? It has been reported that abrogation of the G2/M checkpoint by UCN01 sensitizes p53 defective cells.[24] UCN01 is an anticancer agent (7-hydroxystaurosporine) used to disable the G2/M checkpoint in tumor cells by inhibiting both the cdc25c and Chk1 kinases. In several cancer cell lines, this agent increases the efficacy of chemotherapy and radiotherapy.[25,26] The topoisomerase I Inhibitor BNP1350 induces alteration of the G2 checkpoint kinase Chk1 in human head and neck carcinoma A253 cells.[27] Therefore, one possible approach is to abrogate the G2 arrest in response to DNA damage in STS. Moreover, this therapy offers the possibility of reducing common side-effects of cancer therapy, because normal cells maintain both the G1/S and G2/M checkpoints.

In conclusion, our findings indicate that the G2/M checkpoint pathway is well preserved in STS, that the active state of this pathway contributes to chemotherapeutic resistance in STS, and that targeting this pathway offers potential in the treatment of STS.

ACKNOWLEDGMENTS

This work was supported by a Grant-in-Aid for Encouragement of Young Scientists (to M.K.) from the Ministry of Education, Scientific, Sports and Culture, and CREST Research Project (to M.K.) from Japan Science and Technology Corporation.

REFERENCES

1 Hartwell LH, Kastan MB. Cell cycle control and cancer. *Science* 1994; **266**: 1821–8.
2 Cahill DP, Lenganer C, Yu J *et al.* Mutations of mitotic checkpoint genes in human cancers. *Nature* 1998; **392**: 300–3.
3 Hartwell LH. Defects in a cell cycle checkpoint may be responsible for genomic instability of cancer cells. *Cell* 1996; **71**: 543–6.
4 Hartwell LH, Weinert TA. Checkpoints: controls that ensure the order of cell cycle events. *Science* 1989; **246**: 629–34.
5 Hollstein M, Rice K, Greenblatt MS *et al.* Database of p53 gene somatic mutations in human tumors and cell lines. *Nucl Acid Res* 1994; **22**: 3551–5.

6 Sousai T, Legres Y, Lubin R, Ory K, Schlichtholz B. Multifactorial analysis of p53 alternation in human cancer: a review. *Int J Cancer* 1994; **57**: 1–9.

7 Cordon-Cardo C, Latres E, Drobnjak M *et al.* Molecular abnormalities of mdm2 and p53 genes in adult soft tissue sarcomas. *Cancer Res* 1994; **54**: 794–9.

8 Taubert H, Wurl P, Bache M *et al.* The p53 gene in soft tissue sarcomas: prognostic value of DNA sequencing versus immunohistochemistry. *Anticancer Res* 1998; **18**: 183–8.

9 Blasina A, de Weyer IV, Lans MC, Luyten WH, Parker AE, McGowan CH. A human homologue of the checkpoint kinase Cds1 directly inhibits Cdc25 phosphatase. *Curr Biol* 1999; **9**: 1–10.

10 Sanchez Y, Wong C, Thoma RS *et al.* Conservation of the Chk1 checkpoint pathway in mammals: linkage of DNA damage to Cdk regulation through Cdc25. *Science* 1997; **277**: 1497–501.

11 Bunz F, Dutriaux A, Lengauer C *et al.* Requirement for p53 and p21 to sustain G_2 arrest after DNA damage. *Science* 1998; **282**: 1497–501.

12 Vahteristo P, Tamminen A, Karvinen P *et al.* p53, Chk1, and Chk2 genes in Finnish families with Li–Fraumeni syndrome: further evidence of CHK2 in inherited cancer predisposition. *Cancer Res* 2001; **61**: 5718–22.

13 Miller CW, Ikezoe T, Krug U *et al.* Mutations of the CHK2 gene are found in some osteosarcomas, but are rare in breast, lung, and ovarian tumors. *Genes Chromosomes Cancer* 2002; **33**: 17–21.

14 Matsuoka S, Nakagawa T, Masuda A, Haruki N, Elledge SJ, Takahashi T. Reduced expression and impaired kinase activity of a Chk2 mutant identified in human lung cancer. *Cancer Res* 2001; **61**: 5362–5.

15 Nakajo N, Yoshitome S, Iwashita J *et al.* Absence of Wee1 ensures the meiotic cell cycle in *Xenopus* ocytes. *Genes Dev* 2000; **14**: 328–38.

16 Martinho RG, Lindsay HD, Flaggs G *et al.* Analysis of Rad3 and Chk1 protein kinases defines different checkpoint responses. *EMBO J* 1998; **17**: 7239–49.

17 Allen JB, Zhou Z, Siede W, Friedberg EC, Elledge SJ. The SAD1/RAD53 protein kinase controls multiple checkpoints and DNA damage-induced transcription in yeast. *Genes Dev* 1994; **8**: 2401–15.

18 Graves PR, Lovly CM, Uy GL, Helen PW. Localization of human Cdc25c is regulated both by nuclear export and 14-3-3 protein binding. *Oncogene* 2001; **20**: 1839–51.

19 Powell SN, De Frank JS, Connell P *et al.* Differential sensitivity of p53 (–) and p53 (+) cells to caffeine-induced radiosensization and override of G2 delay. *Cancer Res* 1995; **55**: 1643–8.

20 Yao SL, Akhtar AJ, McKenna KA *et al.* Selective radiosensitization of p53-deficent cells by caffeine-mediated activation of p34cdc2 kinase. *Nat Med* 1996; **2**: 1140–3.

21 Tsuchiya H, Tomita K, Mori Y, Asada N, Yamamoto N. Marginal excision for osteosarcomas with caffeine assisted chemotherapy. *Clin Orthop* 1999; **358**: 27–35.

22 Tomita K, Tsuchiya H. Caffeine enhancement of the effect of anticancer agents on human sarcoma cells. *Jpn J Cancer Res* 1989; **80**: 83–8.

23 Zhou BBS, Chaturvedi P, Spring K *et al.* Caffeine abolishes the mammalian G2/M DNA damage checkpoint by inhibiting ataxia-telangiectasia-mutated kinase activity. *J Biol Chem* 2000; **275**: 10342–8.

24 Luo Y, Rockow-Magnone SK, Joseph MK *et al.* Abrogation of G2 checkpoint specifically sensitizes p53 defective cells to cancer chemotherapeutic agents. *Anti Cancer Res* 2001; **21**: 23–8.

25 Hirose Y, Berger MS, Pieper PO. Abrogation of the Chk1-mediated G2 checkpoint in a pathway potentiates temozolomide-induced toxicity in a p53-independent manner in human glioblastoma cells. *Cancer Res* 2001; **61**: 5843–9.

26 Busby EC, Leistritz DF, Abraham RT, Karnitz LM, Sarkaria JN. The radiosensitizing agent 7-hydroxystaurosporine (UCN01) inhibits the DNA damage checkpoint kinase Chk1. *Cancer Res* 2000; **60**: 2108–12.

27 Yin MB, Guo B, Vanhoefer U *et al.* Characterization of protein kinase chk1 essential for human head and neck carcinoma A253 cells to a novel topoisomerase I inhibitor BNP 1350. *Mol Pharm* 2000; **57**: 453–9.

Virchows Arch (2004) 444:28–35
DOI 10.1007/s00428-003-0889-9

ORIGINAL ARTICLE

Koutaro Shinmura · Tsuyoshi Ishida · Takahiro Goto · Masahiko Kuroda · Hiroyuki Hattori · Shuzou Nagai · Tetsuo Imamura · Kiyoshi Mukai · Atsuhiro Imakiire

Expression of cyclooxygenase-2 in chondroblastoma: immunohistochemical analysis with special emphasis on local inflammatory reaction

Received: 7 April 2003 / Accepted: 28 July 2003 / Published online: 9 September 2003

Abstract To investigate the frequency and mechanism of the peritumoral inflammatory reaction in chondroblastoma, we evaluated the relationship between clinicoradiological findings and immunohistochemical expression of cyclooxygenase-2 (COX-2) in excised tumors. Twenty-one cases of chondroblastoma were studied. Imaging analysis was performed with radiographs and T1- and T2-weighted magnetic resonance images in all cases and with computed tomography scan and bone scintigraphy in some cases. Immunohistochemical study for COX-2 was carried out using formalin-fixed paraffin-embedded tissues. Periosteal reaction was observed in 6 cases (29%) and bone marrow edema in 15 cases (71%). Soft-tissue edema, joint effusion, and synovitis were found in 10 cases (48%), in 7 cases (33%), and in 9 cases (43%), respectively. Immunohistochemical expression of COX-2 in chondroblastoma cells was found in 15 of 21 cases (71%). The intensity of COX-2 immunoreactivity was correlated statistically with the presence of periosteal reaction, bone-marrow edema, soft-tissue edema, and synovitis. Our results indicate that activation of eicosanoid synthesis by COX-2 expression in the tumor itself is probably an important factor, inducing peritumoral inflammatory changes in chondroblastomas.

Keywords Chondroblastoma · Cyclooxygenase-2 · Immunohistochemistry · Inflammation · Radiographs · CT · MRI

K. Shinmura · H. Hattori · S. Nagai · A. Imakiire
Department of Orthopedic Surgery,
Tokyo Medical University,
Nishishinjuku 6-7-1, Shinjuku-ku, 160-0013 Tokyo, Japan

T. Ishida · M. Kuroda · K. Mukai
First Department of Pathology,
Tokyo Medical University,
Shinjuku 6-1-1, Shinjuku-ku, 160-8402 Tokyo, Japan

T. Goto
Department of Orthopaedic Surgery,
Faculty of Medicine, The University of Tokyo,
Hongo 7-3-1, Bunkyo-ku, 113-8655 Tokyo, Japan

T. Imamura
Department of Surgical Pathology,
Teikyo University School of Medicine,
Kaga 2-11-1, Itabashi-ku, 173-8605 Tokyo, Japan

T. Ishida (✉)
First Department of Pathology,
Tokyo Medical University,
Shinjuku 6-1-1, Shinjuku-ku, 160-8402 Tokyo, Japan
e-mail: ishida@tokyo-med.ac.jp
Tel.: +81-33-3516141
Fax: +81-33-3526335

Introduction

Chondroblastoma is a relatively rare benign cartilage tumor, representing approximately 1% of all primary bone tumors [7, 21]. It most frequently occurs in the second decade of life and arises in the epiphysis or apophysis of long tubular bone, especially of the proximal and distal femur, proximal tibia, and proximal humerus. Chondroblastoma is typically a well-demarcated lytic lesion with or without calcification on radiographs.

In some chondroblastoma cases, synovitis and inflammatory reactions around the tumor may be found, and these findings are well demonstrated by different imaging modalities, including magnetic resonance imaging (MRI). MRI is a sensitive imaging modality for demonstrating these inflammatory reactions; thus, MRI may lead to overestimation of the aggressiveness and extent of the tumor. Knowledge of the potential pitfalls may help to avoid misplaced reliance on MRI for benign bone tumor diagnosis [12]. Some chondroblastoma tissues contain high levels of prostaglandins (PGs), which are considered to play an important role in the development of a peritumoral inflammatory reaction revealed by imaging studies [25]. PGs are produced from phospholipids via arachidonic acid metabolism by cyclooxygenase-2 (COX-2). Thus, we sought to examine the expression of COX-2

in chondroblastoma tissue and to evaluate the relationship between COX-2 expression and the inflammatory reaction of the peritumoral tissues in chondroblastomas.

Materials and methods

Tumor samples

We retrieved 21 cases of chondroblastoma from the files of Division Surgical Pathology, Tokyo Medical University Hospital; Department of Pathology, Teikyo University School of Medicine; and Department of Pathology, The University of Tokyo Hospital. Treatment was curettage in all but two of these cases, and it was en-block excision in these two cases. The histopathological diagnosis of each tumor was re-confirmed by two of the authors (T. Is. and T. Im.) according to the criteria described in the bone tumor textbooks [7, 21].

Clinical and imaging studies

Clinical symptoms were evaluated for signs and symptoms of local inflammation, including the presence of local pain, swelling, limitation in range of motion in the adjacent joint, and muscle atrophy of affected limb. In all cases, plain radiographs and T1- and T2-weighted MRI were available for review. Tomogram, computed tomography (CT) scan, and bone scintigram were also examined in some cases. MRI was obtained using either a 0.5- or 1.5-T unit prior to surgery. MRI techniques, however, were not tightly controlled because of the different scanners available at the different institutes examined in this study. A range of spin-echo pulse sequences was obtained for T1- and T2-weighted images. Gadolinium-labeled diethylene triamine pentaacetate (Gd-DTPA)-enhanced T1-weighted images were obtained in 15 cases. The presence of a periosteal reaction was evaluated by radiographs, tomograms, and CT scans. Bone-marrow edema, soft-tissue swelling and edema, joint effusion, and synovitis were evaluated on MRI. Bone marrow demonstrating lower signal intensity than normal marrow intensity on T1-weighed images as well as high signal intensity on T2-weighed images was considered positive for intramedullary bone-marrow edema [19, 22]. For joint effusion, accumulation of joint fluid that is clearly demonstrated in the joint space adjacent to the tumor as high signal intensity on T2-weighed images was considered a positive finding. Synovitis and soft-tissue swelling and edema were defined as tissue swelling with high signal intensity on T2-weighted images or on Gd-DTPA-enhanced T1-weighted images [1, 9].

Histological and immunohistochemical studies

Tumor tissues were fixed in 10% formalin and embedded in paraffin. Histological sections were cut at 3 μm thickness and stained with hematoxylin and eosin. Immunohistochemical study was carried out by the labeled streptavidin biotin (LSAB) method using LSAB kit (Dako, Capinteria, CA). Polyclonal antibody for COX-2 (IBL; Fujioka, Japan, dilution 1:50) was used for primary antibody. Deparaffinized sections were incubated in methanol with 0.3% hydrogen peroxide to eliminate endogenous peroxidase activity. Antigen retrieval method was applied with autoclaving at 110°C for 10 min in 10 mM citrate buffer (pH 6.0). Colorectal adenocarcinoma tissue known to express COX-2 was used as a positive control. As the negative control, the primary antibody was replaced with Tris-NaCl buffer. The results of immunoreactivity were divided into four grades according to the number of positive cells, i.e., negative staining (0–9%), 0; weak staining (10–29%), 1+; moderate staining (30–49%), 2+; strong staining (50%>), 3+. In three cases, the synovial tissue adjacent to the tumor was also examined histologically and immunohistochemically. Immunohistochemical evaluation in 20 cases of giant cell tumor (GCT) (14 male and 6 female, age range 20–75 years, mean age 33 years) of bone in the epiphysis of the long bones (location as follows: proximal tibia, 7 cases; distal femur, 6 cases; distal radius, 3 cases; proximal humerus, 2 cases; sacrum and acetabulum, 1 case each) other than two cases was performed in comparison with chondroblastomas.

Statistical analysis

Correlation between the grading of COX-2 expression and inflammatory reactions was tested by the Spearman's correlation coefficient by rank test. Statistical significance was defined as $P<0.05$.

Results

In the 21 cases examined (7 male and 14 female; age range 11–35 years), the location of the tumor was the proximal femur (7 cases), distal femur (3 cases), proximal humerus (7 cases), proximal tibia (2 cases), and acetabulum and calcaneus (1 case each). Although local pain was a common complaint, details of pain relief from NSAIDs were unknown.

Clinical symptoms and radiological features

Clinical data are summarized in Table 1. Symptoms considered indicative of inflammation were observed. Local pain and limitation in range of motion in the affected joint were observed in 20 (95%) and 15 (71%) cases, respectively. Muscle atrophy of affected limb was recognized in 10 cases (48%), which had a substantial impairment of movement caused by pain. In preoperative laboratory data, a slight increase of white blood cells was seen in only one case. C-reactive protein was within normal limits in all cases.

Imaging findings of tumors studied were all well-circumscribed radiolucent lesion with a sclerotic rim (Fig. 1, Fig. 2). Calcification, punctuated or flocculant, was found in 12 cases (57%). Cystic changes demonstrated by MRI were found in 12 cases (57%). Interruption of the cortex was noted on CT scan in 10 cases (48%).

On plain radiograph, a periosteal reaction was observed in 6 cases (29%). The affected anatomical locations of these periosteal reaction-positive cases were all long tubular bone. Specifically, the location of the tumor in 4 of 6 cases was the proximal humerus. The femur and tibia were the site of the lesion in one case each. In 5 cases, a distinctive layered-type periosteal reaction along the diametaphyeal shaft distant from the tumor was recognized. In the remaining 1 case, remarkable periosteal reaction of solid buttressing type was seen along the proximal shaft of the humerus (Fig. 1). Bone-marrow edema was revealed in 15 cases (71%). The extent of edema varied from slight to prominent, and tended to localize to marrow space distant from original tumors (Fig. 1B, C, D, Fig. 2A, B). Soft-tissue edema was revealed, extending to peritumoral muscles in 10 cases (48%) and was seen in 5 of the 7 cases affecting in the

Table 1 Summary of clinical symptoms, imaging findings, and immunohistochemical cyclooxygenase-2 (COX-2) expression. *ROM* range of motion, *GT* greater trochanter, *0* negative staining, *1+* weak staining, *2+* moderate staining, *3+* strong staining

Case no.	Age/sex	Location	Clinical symptoms				Inflammatory reactions in images					COX-2 expression
			Local pain	Swelling	Limitation of ROM	Muscle atrophy	Periosteal reaction	Bone-marrow edema	Soft-tissue edema	Joint effusion	Synovitis	
1	11 years/female	Humerus (proximal)	+	+	+	+	+	+	+	–	+	3+
2	26 years/female	Femur (GT)	+	–	–	–	–	+	–	–	–	1+
3	19 years/female	Acetabulum	+	–	+	+	–	–	–	–	–	0
4	20 years/male	Humerus (proximal)	+	+	+	–	+	+	+	+	+	1+
5	21 years/male	Humerus (proximal)	+	+	+	–	–	–	–	–	–	0
6	11 years/female	Humerus (proximal)	+	+	+	+	–	+	+	–	–	1+
7	16 years/male	Tibia (proximal)	–	+	+	–	+	+	+	–	+	2+
8	16 years/male	Humerus (proximal)	+	+	+	–	+	+	+	–	–	3+
9	35 years/male	Calcaneus	+	–	–	–	–	+	–	–	–	0
10	20 years/female	Femur (head)	+	–	–	–	–	–	–	–	–	0
11	15 years/male	Tibia (proximal)	+	–	–	+	–	–	–	–	–	1+
12	27 years/female	Femur (head)	+	–	+	–	–	+	+	+	+	1+
13	19 years/female	Femur (distal)	+	+	–	–	–	+	+	+	+	1+
14	13 years/male	Humerus (proximal)	+	–	+	+	–	+	+	+	+	2+
15	13 years/female	Femur (distal)	+	+	+	+	+	+	–	–	–	1+
16	11 years/female	Femur (distal)	+	+	+	+	–	+	–	+	+	2+
17	19 years/female	Femur (GT)	+	–	–	–	–	–	–	–	–	0
18	15 years/female	Femur (Head)	+	–	+	+	–	+	+	+	+	3+
19	15 years/female	Humerus (proximal)	+	+	+	+	+	+	–	–	–	3+
20	17 years/female	Femur (head)	+	–	+	–	–	–	–	–	–	0
21	15 years/female	Femur (head)	+	–	+	+	–	+	+	+	+	3+

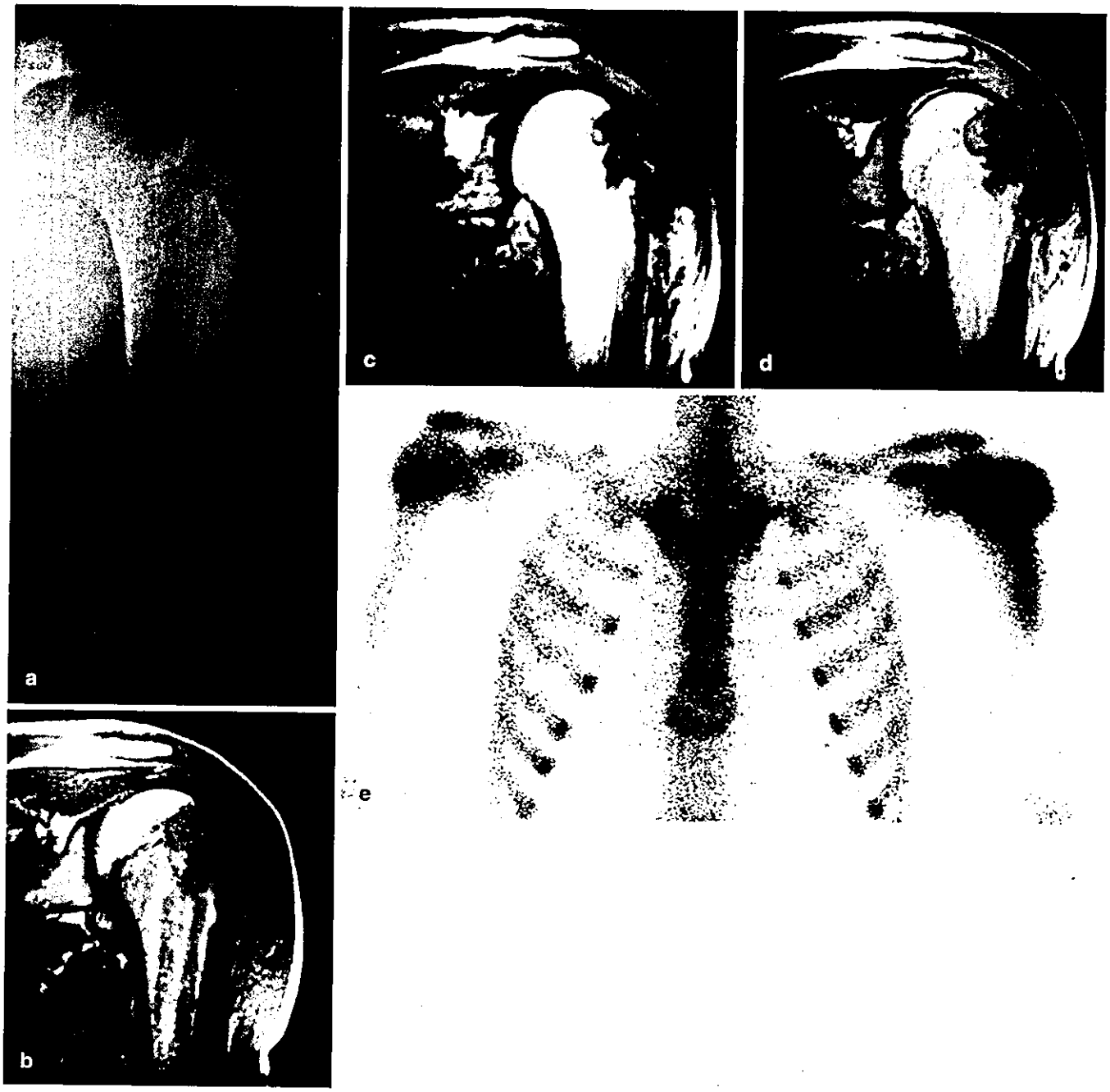

Fig. 1 **A** A plain radiograph of the humerus shows a well-circumscribed calcified tumor of the epiphysis with conspicuous periosteal reaction of solid buttressing type along the diametaphyseal shaft far from the tumor (case no. 8). **B** Coronal T1-weighted magnetic resonance (MR) image [repetition time (TR)/echo time (TE): 450/25] reveals a protruding tumor showing intermediate to low signal intensity. Bone-marrow edema is also identified as a longitudinal area of low signal intensity descending into the diaphyseal shaft. **C** Coronal T2-weighted MR image (TR/TE: 3000/100) reveals a low signal intensity tumor and bone-marrow edema showing high signal intensity. **D** Gadolinium-labeled diethylene triamine pentaacetate-enhanced T1-weighted image reveals bone-marrow edema as an area of high signal intensity and soft-tissue edema in the rotator cuff and deltoid muscle around the tumor. **E** Bone scintigram shows intense uptake in the proximal humerus and also less intense uptake along the lateral shaft far beyond the tumor itself

proximal humerus. Joint effusion had various patterns from slight to extreme in 7 cases (33%) and was seen in 3 of the 5 cases affecting in the femoral head (Fig. 2A, B). Synovitis was found in only 9 cases (43%) (Fig. 2A, B).

Immunohistochemical study

The histology of the tumors demonstrated findings typical of chondroblastoma, with sheet-like proliferation of round-shaped chondroblasts and foci of chondroid matrix

Fig. 2 A Coronal T1- weighted image (TR/TE: 500/17) reveals a well-demarcated tumor with isointensity and bone-marrow edema showing low signal intensity in the intertrochanteric area (case no. 18). **B** Coronal T2-weighted image (TR/TE: 3000/96) reveals bone-marrow edema with high signal intensity in the corresponding area of T1-weighted image and obvious joint effusion (*large arrows*) and synovitis (*small arrows*) in affected side. The tumor shows low signal intensity

production associated with occasional chicken-wire calcification and scattered osteoclast-like giant cells (Fig. 3A). These findings were observed in all cases in most areas, or at least within the focal area of tumors studied. Synovial tissue studied in three cases showed reactive synovitis with hyperemia, edema, and lymphoplasmacytic infiltration (Fig. 3B).

The results of immunohistochemical study are summarized in Table 1. Of 21 tumors, 15 (71%) were positive for COX-2 (Fig. 3C, D). The staining intensity was unequivocally positive among all COX-2-positive cases. In contrast, three samples of synovial tissue of the affected joint and all 20 GCT did not express COX-2. In 15 COX-2-positive cases, 7 cases showed only weak staining (1+), but 3 cases showed moderate staining (2+). In the remaining 5 cases, multiple foci of COX-2-positive tumor cells were observed, and they were classified as strong staining (3+). The expression of COX-2 was found in both areas of cellular sheet of tumor cells and tumor cells embedded in the chondroid matrix. There was no change of staining property among chondroblasts and cells within the cartilage matrix. Osteoclast-like giant cells were consistently negative for COX-2. There was no correlation of histological features (mitotic activity, apoptosis, tumor vessel formation, and tumor size) except inflammatory reactions and COX-2 expression.

Statistical analysis

The grading of COX-2 immunoreactivity was correlated with the presence of periosteal reaction (P=0.035), bone-marrow edema (P<0.01), soft-tissue edema (P=0.037), and synovitis (P=0.015).

Discussion

In general, radiological images correspond well with the aggressiveness of bone tumors. Radiographically, non-aggressive tumors showed bland-looking appearances without periosteal reaction, cortical violation, and adjacent tissue inflammation. These entities usually contain benign tumors and tumor-like lesions. However, aggressive lesions, such as malignant bone tumors, some osteomyelitis, and eosinophilic granuloma, induce tissue reactions adjacent to the lesions. These reactions include a periosteal reaction, bone-marrow and soft-tissue edema, synovial fluid accumulation, and soft-tissue swelling. In some benign tumors, however, these prominent tissue reactions, which are normally associated with aggressive or malignant bone lesions, have been described [12]. Osteoid osteoma is a typical example of such a benign tumor [17, 18]. Recent imaging advances, especially MRI, have revealed that other benign tumors, e.g., chondroblastomas, demonstrate tissue reactions around them[3, 12, 16, 23, 25].

In general, chondroblastoma shows a well-circumscribed radiolucent lesion with or without calcification and sclerotic rim. In addition to these findings, inflammatory responses, including periosteal reaction, bone-marrow and soft-tissue edema, and synovitis, have been described in some chondroblastomas by plain film or MRI. A thick-solid or layered-type periosteal reaction distant from the lesion itself has been found in 20–90% of cases of chondroblastoma on radiography or MRI [2, 3, 4, 8, 12, 13, 15, 16, 23, 25]. Bone-marrow edema extending to the circumference of the tumor is observed in 82–92% of cases on MRI, and soft-tissue edema is also found in 58–82% of cases [15, 16, 23]. Approximately 30% of cases are associated with joint effusion as demonstrated by MRI [15, 16, 25]. In our study, the frequency of inflammatory reaction was similar to previously reported data. Periosteal reaction was noted in 29%, bone-marrow edema in 71%, soft-tissue edema in 48%, joint effusion in 33%, and synovitis in 43% of cases examined. Therefore, the frequencies of inflammatory reactions found in chondroblastoma cases appear to be consistent across institutions.

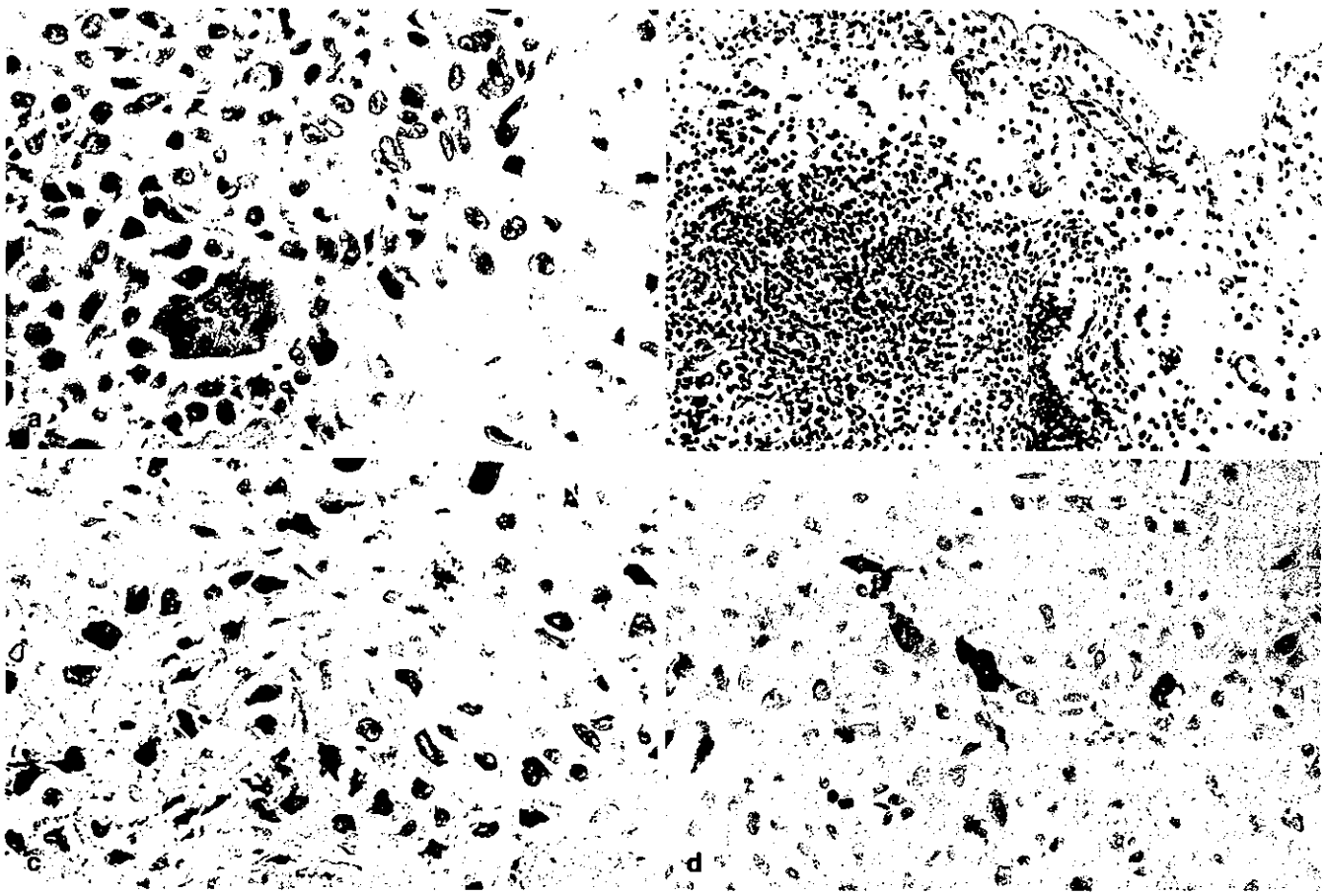

Fig. 3 **A** Histology of the tumor shows sheet-like proliferation of chondroblasts and chondroid matrix production (case no. 18) (hematoxylin and eosin, ×100). **B** Histology of synovium shows reactive synovitis with edema, hyperemia, and lymph follicle (case no. 21) (hematoxylin and eosin, ×50). **C–D** Immunohistochemical staining for cyclooxygenase-2 (COX-2). **C** The tumor cells are diffusely positive for COX-2 in (3+) case (case no. 8) (×100). **D** COX-2 expression is seen in (1+) case (case no. 2) (×100)

The mechanism of inflammatory reactions that are sometimes observed in benign bone tumors remains unclear. Recent studies suggest, however, that high levels of PGs within the lesion, such as osteoid osteoma and chondroblastoma, may play an important role for the development or maintenance of inflammatory reactions [5, 10, 11, 24, 26].

COX is the essential regulatory enzyme of the eicosanoid biosynthetic pathway and catalyzes the conversion of arachidonic acid into PGG2 and PGH2. PGH2 is subsequently converted into various eicosanoids including PGE2, PGF2α, PGI2, and the like. COX has two different isoforms, COX-1 and COX-2, derived from distinct genes, respectively. COX-1 is constitutively expressed and mediates many of the housekeeping functions of COX in nearly all tissues under basal conditions [6]. Conversely, COX-2 is inducible and is considered to be a key mediator of inflammation via the eicosanoid biosynthetic pathway.

In osteoid osteomas, PGs are thought to be responsible for inflammatory reactions around the nidus and for nocturnal pain that is characteristically relieved by nonsteroidal anti-inflammatory drugs (NSAIDs). Osteoblastic tumor cells within the osteoid osteoma nidus have shown diffuse immunoreactivity for COX-2 [17, 18, 20]. Bone-marrow edema around the lesion detected by MRI is greatly reduced or eliminated after surgical removal of the nidus [18]. Taken together, these data suggest that COX-2 expression in osteoid osteoma cells may play a major role in activating the eicosanoid biosynthetic pathway leading to bone-marrow edema and other inflammatory reactions found in osteoid osteoma cases.

In our study, immunohistochemical expression of COX-2 in chondroblastoma cells was found in 15 of 21 cases (71%). Osteoclastic giant cells and synovial tissue and osteoblasts around the lesion were all negative for COX-2. Bone-marrow edema was observed in 14 of 15 COX-2-positive cases; however, only 1 case was observed in which COX-2 staining was negative and bone-marrow edema was present. COX-2 expression is seen in all periosteal reaction-, joint effusion-, synovitis-, and soft-tissue edema-positive cases. No cases were seen with negative COX-2 staining that were positive for periosteal reaction, joint effusion, synovitis, or soft-tissue edema. These observations indicate that COX-2 expression in tumor tissue and inflammatory reactions are closely

related and are statistically significant. In addition, a small COX-2-positive chondroblastoma (case no.13) was also associated with these inflammatory reactions [14]. Conversely, in relatively large, COX-2-negative chondroblastomas, the inflammatory reactions are not found. Thus, it appears that the most important factor for inducing inflammatory reactions in chondroblastoma is COX-2 expression in the lesion itself, most likely via activation of eicosanoid biosynthetic pathway. The study of PG concentration in chondroblastoma is limited; however, Wold et al. demonstrated that one chondroblastoma tumor sample contained increased levels of PGE2 relative to the adjacent bone [24]. Another study reported by Yamamura et al. showed higher levels of PGs in eight cases of chondroblastoma than that of other cartilage tumors and GCT [26].

In osteoid osteoma, diffuse intense immunoreactivity for COX-2 was found in osteoblastic tumor cells [17, 18, 20]. COX-2 immunoreactivity in chondroblastomas was less intense than in typical cases of osteoid osteoma [14]. Among chondroblastoma cases, intensity of COX-2 expression may also correlate with the intensity of peritumoral inflammatory reactions, but does not correlate with tumor size.

Bone-marrow edema is more frequently seen than other peritumoral inflammatory changes. This could be related to the fact that bone marrow is adjacent to the tumor and that MRI is a very sensitive imaging modality. The periosteum, synovium, and joint cavity are not close to the tumor itself; therefore, the concentration of PGs in these tissues is likely lower than within the bone marrow immediately surrounding the lesion. In addition, plain radiography and CT are less sensitive imaging modalities for the detection of periosteal reaction.

GCT is an aggressive tumor that generally occurs in the epiphysis like chondroblastoma. Despite histological similarities, these two entities must be distinguished because of their radically different biological behavior. Although local aggressiveness is frequently observed in giant cell tumor, peritumoral inflammatory changes have not been noted in giant cell tumor. Interestingly, all 20 cases of giant cell tumor studied show neither COX-2 immunoreactivity nor inflammatory reactions. Thus, peritumoral inflammatory reactions are not related to tumor histology, size, location, and aggressiveness, but are related to COX-2 expression in the tumor tissue.

In summary, there is the possibility that increased COX-2 expression is only an associated finding with inflammation; nevertheless, our study suggests that COX-2 expression is likely an important factor for inducing peritumoral inflammatory changes in chondroblastomas. The same mechanism, activation of eicosanoid biosynthetic pathway by COX-2 within the tumor, functions in these secondary inflammatory reactions, such as bone-marrow edema and periosteal reaction both in the chondroblastoma and osteoid osteoma.

References

1. Beltran J, Chandnani V, McGhee RA Jr, Kursunoglu-Brahme S (1991) Gadopentetate dimeglumine-enhanced MR imaging of the musculoskeletal system. Am J Roentgenol 156:457–466
2. Bloem JL, Mulder JD (1985) Chondroblastoma: a clinical and radiological study of 104 cases. Skeletal Radiol 14:1–9
3. Braunstein E, Martel W, Weatherbee L (1979) Periosteal bone apposition in chondroblastoma. Skeletal Radiol 4:34–36
4. Brower AC, Moser RP, Kransdorf MJ (1990) The frequency and diagnostic significance of periostitis in chondrobalstoma. Am J Roentgenol 154:309–314
5. Ciabattoni G, Tramburrelli F, Greco F (1991) Increased prostacyclin biosynthesis in patients with osteoid osteoma. Eicosanoids 4:165–167
6. Crofford LJ (1997) COX-1 and COX-2 tissue expression: implications and predictions. J Rheumatol 24:15–19
7. Dorfman HD, Czerniak B (eds) (1998) Benign cartilage tumors. In: Bone tumors. Mosby, St. Louis, pp 253–352
8. Edel G, Ueda Y, Nakanishi J, Brinker KH, Roessner A, Blasius S, Vestring T, Muller-Miny H, Erlemann R, Wuisman P (1992) Chondroblastoma of bone. Virchows Archiv 421:355–366
9. Erlemann R, Reiser MF, Peters PE, Vasallo P, Nommensen B, Kusnierz-Glaz CR, Ritter J, Roessner A (1989) Musculoskeletal neoplasms: static and dynamic Gd-DTPA-enhanced MR imaging. Radiology 171:767–773
10. Greco F, Tamburrelli F, Ciabattoni G (1991) Prostaglandins in osteoid osteoma. Int Orthopaedics 15:35–37
11. Hasegawa T, Hirose T, Sakamoto R, Seki K, Ikata T, Hizawa K (1993) Mechanism of pain in osteoid osteomas: an immunohistochemical study. Histopathology 22:487–491
12. Hayes CW, Conway WF, Sundaram M (1992) Misleading aggressive MR imaging appearance of some benign musculoskeletal lesions. Radiographics 12:1119–1134
13. Hudson TM, Hawkins IF Jr (1981) Radiological evaluation of chondroblastoma. Radiology 139:1–10
14. Ishida T, Goto T, Motoi N, Mukai K (2002) Intracortical chondroblastoma mimicking intra-articular osteoid osteoma. Skeletal Radiol 31:603–607
15. Jee WH, Park YK, McCauley TR, Choi KH, Ryu KN, Suh JS, Suh KJ, Cho JH, Lee JH, Park JM, Lee YS, Ok IY, Kim JM (1999) Chondroblastoma: MR characteristics with pathologic correlation. J Comput Assist Tomogr 23:721–726
16. Kaim AH, Hugli R, Bonel HM, Jundt G (2002) Chondroblastoma and clear cell chondrosarcoma: radiological and MRI characteristics with histopathological correlation. Skeletal Radiol 31:88–95
17. Kawaguchi Y, Sato C, Hasegawa T, Oka S, Kawahara H, Norimatsu H (2000) Intraarticular osteoid osteoma associated with synovitis: a possible role of cyclooxygenase-2 expression by osteoblasts in the nidus. Mod Pathol 13:1086–1091
18. Kawaguchi Y, Hasegawa T, Oka S, Sato C, Arima N, Norimatsu H (2001) Mechanism of intramedullary high intensity area on T2-weighted magnetic resonance imaging in osteoid osteoma: a possible role of COX-2 expression. Pathol Int 51:933–937
19. Moore SG, Bisset GS 3rd, Siegel MJ, Donaldson JS (1991) Pediatric musculoskeletal MR imaging. Radiology 179:345–360
20. Mungo DV, Zhang X, O'Keefe RJ, Rosier RN, Puzas JE, Schwarz EM (2002) COX-1 and COX-2 expression in osteoid osteomas. J Orthopaedic Res 20:159–162
21. Unni KK (ed) (1996) Benign chondroblastoma. In: Dahlin's bone tumors: general aspects and data on 11,087 cases, 5th edn. Lippincott-Raven, Philadelphia, pp 47–57
22. Vogler JB 3rd, Murphy WA (1988) Bone marrow imaging. Radiology 168:679–693
23. Weatherall PT, Maale GE, Mendelsohn DB, Sherry CS, Erdman WE, Pascoe HR (1994) Chondroblastoma: classic and confusing appearance at MR imaging. Radiology 190:467–474

24. Wold LE, Pritchard DJ, Bergert J, Wilson DM (1988) Prostaglandin synthesis by osteoid osteoma and osteoblastoma. Mod Pathol 1:129–131
25. Yamamura S, Sato K, Sugiura H, Iwata H (1996) Inflammatory reaction in chondroblastoma. Skeletal Radiol 25:371–376
26. Yamamura S, Sato K, Sugiura H, Katagiri H, Ando Y, Futatsu H, Iwata H (1997) Prostaglandin levels of primary bone tumor tissues correlate with peritumoral edema demonstrated by magnetic resonance imaging. Cancer 79:255–261

Available online at www.sciencedirect.com
SCIENCE DIRECT
ELSEVIER
Cancer Letters xx (2004) 1–8
CANCER Letters
www.elsevier.com/locate/canlet

Effects of 3-methylcholanthrene on the transcriptional activity and mRNA accumulation of the oncogene *hWAPL*

Masahiko Kuroda[a,b,c,*], Kosuke Oikawa[a,b,c], Keiichi Yoshida[a,c], Aya Takeuchi[d], Masaru Takeuchi[d], Masahiko Usui[d], Akihiro Umezawa[c,e], Kiyoshi Mukai[a]

[a]*Department of Pathology, Tokyo Medical University, 6-1-1 Shinjuku, Shinjuku-ku, Tokyo 160-8402, Japan*
[b]*CREST Research Project, Japan Science and Technology Corporation, 4-1-6 Kawaguchi, Saitama 332-0012, Japan*
[c]*Shinanomachi Research Park, Keio University, 35 Shinanomachi, Shinjuku-ku, Tokyo 160-8582, Japan*
[d]*Department of Ophthalmology, Tokyo Medical University, 6-7-1 Nishi-shinjuku, Shinjuku-ku, Tokyo 160-0023, Japan*
[e]*National Research Institute for Child Health and Development, 3-35-31 Taishido, Setagaya-ku, Tokyo 154-8567, Japan*

Received 28 April 2004; received in revised form 26 July 2004; accepted 5 August 2004

Abstract

hWAPL is a human oncogene associated with uterine cervical cancer. Here, we demonstrate that *hWAPL* transcription is induced by 3-methylcholanthrene (3-MC) in the cervical carcinoma-derived cell line SiHa. *hWAPL* transcription was analyzed with evaluation of the mRNA and heterogeneous nuclear RNA (hnRNA) levels by quantitative real time PCR analysis. Flow cytometric analysis suggested that the alteration of *hWAPL* mRNA levels is independent of cell cycle profile. We also found that DMSO and some components of FBS affect *hWAPL* transcription. Interestingly, when the aryl hydrocarbon receptor (AhR) function was inhibited by α-naphthoflavone (ANF), the induction of *hWAPL* transcription by 3-MC was greater than that in AhR-functioning normal cells. These observations suggest that there are complex mechanisms regulating the transcription of *hWAPL*. Furthermore, mRNA level of a mouse homolog of *hWAPL* in mouse uterus was induced by 3-MC injection into the abdominal cavity. Thus, some effects from 3-MC exposure on uterus may be mediated by the unscheduled overexpression of *hWAPL*.

Keywords: 3-Methylcholanthrene (3-MC); hWAPL; Uterine cervical cancer; Aryl hydrocarbon receptor (AhR); α-naphthoflavone (ANF)

1. Introduction

Previously, we have isolated and characterized a novel human gene termed *hWAPL* [1]. Our initial observations suggested that *hWAPL* expression is associated with uterine cervical cancer, although the mechanism was not clear. *hWAPL* is the human homolog of the *wings apart-like* (*wapl*) gene in

* Corresponding author. Address: Department of Pathology, Tokyo Medical University, 6-1-1 Shinjuku, Shinjuku-ku, Tokyo 160-8402, Japan. Tel.: +81 3 3351 6141x425; fax: +81 3 3352 6335.
E-mail address: kuroda@tokyo-med.ac.jp (M. Kuroda).

0304-3835/$ - see front matter © 2004 Published by Elsevier Ireland Ltd.
doi:10.1016/j.canlet.2004.08.006